Article

Biogeochemical Response of the Water Column of Concepción Bay, Chile, to a New Regime of Atmospheric and Oceanographic Variability

Luis Bustos-Espinoza [1], Patricio Torres-Ramírez [1,2], Sergio Figueroa [1], Pablo S. González [1,3], Marcelo A. Pavez [1], Rodolfo Jerez [1], Gonzalo S. Saldías [4,5,6], Claudio Espinoza [1] and Alexander Galán [1,5,7,*]

[1] Centro Regional de Estudios Ambientales (CREA), Universidad Católica de la Santísima Concepción, Concepción 4270789, Chile; lbustos@ucsc.cl (L.B.-E.); ptorres@ucsc.cl (P.T.-R.); sfigueroa@ucsc.cl (S.F.); pablogonzalez@ucsc.cl (P.S.G.); mpavez@ucsc.cl (M.A.P.); cespinozam@ucsc.cl (C.E.)

[2] Programa de Doctorado en Ciencias con Mención en Biodiversidad y Biorecursos, Facultad de Ciencias, Universidad Católica de la Santísima Concepción, Concepción 4060002, Chile

[3] Programa de Doctorado en Ciencias Ambientales con Mención en Sistemas Acuáticos Continentales, Facultad de Ciencias Ambientales, Universidad de Concepción, Concepción 4070409, Chile

[4] Departamento de Física, Facultad de Ciencias, Universidad del Bío-Bío, Concepción 4051381, Chile; gsaldias@ubiobio.cl

[5] Instituto Milenio en Socio-Ecología Costera (SECOS), Santiago 8331150, Chile

[6] Centro de Investigación Oceanográfica COPAS COASTAL, Universidad de Concepción, Concepción 4070409, Chile

[7] Centro de Investigación de Estudios Avanzados del Maule (CIEAM), Vicerrectoría de Investigación y Postgrado and Departamento de Obras Civiles, Facultad de Ciencias de la Ingeniería, Universidad Católica del Maule, Talca 3480112, Chile

* Correspondence: agalan@ucm.cl; Tel.: +56-9-87407150

Abstract: Concepción Bay is a socio-economic and ecologically important embayment whose hydrographic variability has been historically regulated by wind-modulated seasonal upwelling events during spring–summer and by freshwater from precipitation and river discharges during fall–winter. This system is subject to several anthropogenic and environmental strains due to the intense port activity and the increasing occurrence of extreme natural events. This study determines a new hydrographic regime and characterizes and analyzes the biogeochemical response of the water column to changes in rainfall and upwelling patterns. Despite the intrusion of nitrate-rich upwelled waters that enhance biological productivity remains more intense during spring–summer, the system remains fertilized year-long due to the occurrence of persistent upwelling pulses during fall–winter. The hydrographic structure presented a two-layer water column that was stratified thermally in spring–summer and primarily by freshwater inputs in fall–winter. Nevertheless, the regular pattern of the rainfall has changed (a decrease in precipitation and an increased frequency of extreme rainfall events), together with recurrent upwelling-favorable wind pulses during the non-upwelling season. This new regime has altered the seasonality of the physicochemical conditions and the structure of the microplanktonic communities, with productive and sanitary implications affecting the biogeochemical status of CB.

Keywords: Concepción Bay; coastal upwelling; extreme rainfall; new hydrographic regime; biogeochemistry; phytoplankton; pelagic

1. Introduction

Concepción Bay (CB) is a semi-enclosed and shallow (maximum depth is ~45 m) embayment located in the inner part of the widest continental shelf off central-southern Chile (35°42′ S–73°0.3′ W). It is an important socio-economic and ecological ecosystem, mainly because of the port industry but also because of tourism, gastronomy, hotels, sports

activities, and the exploitation of marine resources. From the ecological perspective, a pivotal feature of this highly productive system is the larvae retention of many commercial species and the harboring of some protected areas for the cultivation and exploitation of several species of macroalgae and mollusks [1–5].

In general, alongshore equatorward winds in eastern ocean boundaries promote coastal upwelling, a process modulated by the earth´s rotation (the Coriolis force deflecting fluid motion to the left in the southern hemisphere) and the wind stress forcing. As a result, nutrient-rich, deeper waters are advected to the nearshore area, fertilizing the euphotic zone. In this sense, CB is a highly productive system (3.50–5.75 g C m^{-2} d^{-1}) [6–8] historically characterized by a wind-modulated seasonal injection of high-nutrient, oxygen-deficient Equatorial Subsurface waters (ESSW) that are upwelled into the bay during austral spring and summer [6]. Changes to northerly winds during fall and winter promote the entrance of highly oxygenated and nutrient-poor sub-Antarctic waters (SAAW) [6,9,10], that are eventually diluted at the surface by freshwater input due to the high rainfall and river runoff. The current knowledge indicates that the downwelling produced during fall–winter breaks down the stratification, mixing the entire water column [6].

CB experienced an important industrial development during the 1960s. However, since the 1980s, when this coastal area sustained the most significant development of the country, in concomitance with an increased population and urban growth, this embayment has maintained an accelerated and sustained environmental degradation, especially due to pollution [11–13] and eutrophication processes [14,15]. In this sense, domestic and industrial wastes are discharged (directly and indirectly) into the bay through the Rocuant saltmarsh, Andalien river, Bellavista creek, and a couple of submarine outfalls with just a primary treatment or directly without treatment through diffuse sources, with several sanitary issues affecting not just the environmental quality but also the public health [16–18]. In fact, the port of Talcahuano, located in the southwest area of the bay, was declared one of the most contaminated coastal sites in the world by the Environmental Protection Agency of the US (EPA) because of the high load of organic matter and pollutants in the sediments [19].

Since the industrial revolution, on the other hand, exponential increments in average global temperature from 0.8 to 1.2 °C have caused significant impacts on the frequency and intensity of weather events, hindering their predictability [20]. For instance, increases in the recurrence of forest fires and desiccation events, together with early spring snow melts, have been reported worldwide [21,22]. Concomitantly, changes in the frequency, intensity, and timing of extreme rainfall events (i.e., the number of events per unit time with intensity above a given threshold) are becoming more recurrent and less spatially and seasonally predictable [23,24]. It is well established that the intensity of these extreme precipitation events increases more strongly with changes in global mean surface temperature than mean precipitation [25–29], being recognized as some of the major threats of climate change [30]. Actually, based on observations and climate models, Myhre et al. [31] found that, if historical trends continue, not just the strength but also the occurrence of these intense events would almost double for each degree of further global warming. Furthermore, in the context of this climate crisis [20], several ocean threats have also been projected, which have already begun to become evident, such as the decrease in seawater oxygen concentrations [32] and increase in water column stratification [33], as well as coastal eutrophication [34], together with an intensification of the upwelling process in response to the strengthening of the alongshore wind stress along eastern boundaries [35,36].

Despite the ecological importance of CB and its being impacted by several anthropogenic and natural climatic stressors, this ecosystem has been poorly studied recently. Here, we evaluated the historical variability of rainfall and Ekman transport, and through seasonal sampling, the biogeochemical response of the water column of CB to the new atmospheric and oceanographic regimes was determined. We postulate that the decrease in the supply of freshwater as a result of the extreme drought that has affected the region since 2009 and changes in the frequency, seasonality, and intensity of both the rainfall pattern

and the upwelling-favorable wind pulses have altered the marked seasonal pattern. As a result, the temporal behavior of physicochemical conditions and the size structure of microplanktonic communities have changed, impacting the functioning of the ecosystem.

2. Materials and Methods

2.1. Study Site and Sample Collection

Concepción Bay is a semi-enclosed coastal embayment of 167.4 km^2, located at 35°42′ S–73°0.3′ W, and distinguished by its north–south orientation that enhances a marked seasonal wind-modulated change in its circulation pattern [37]. Seasonal sampling was carried out on board the R/V Don Antonio during the austral summer (3–4 January), fall (30–31 May), winter (29–30 August), and spring (29–30 November) of 2018. Eight stations were sampled to cover the greatest variability of the bay (e.g., marine influence—St. 1 and 2, tributaries—St. 4 and 7, and wetlands—St. 8), as well as zones of large anthropogenic impact (e.g., port activities—St. 5 and 7, ship refueling—St. 6, and influence of outfalls—St. 7)—see Figure 1. Sampling information, including dates and the parameters evaluated, is summarized in Table 1, whereas the positions and depths of sampling at each station are shown in Table 2.
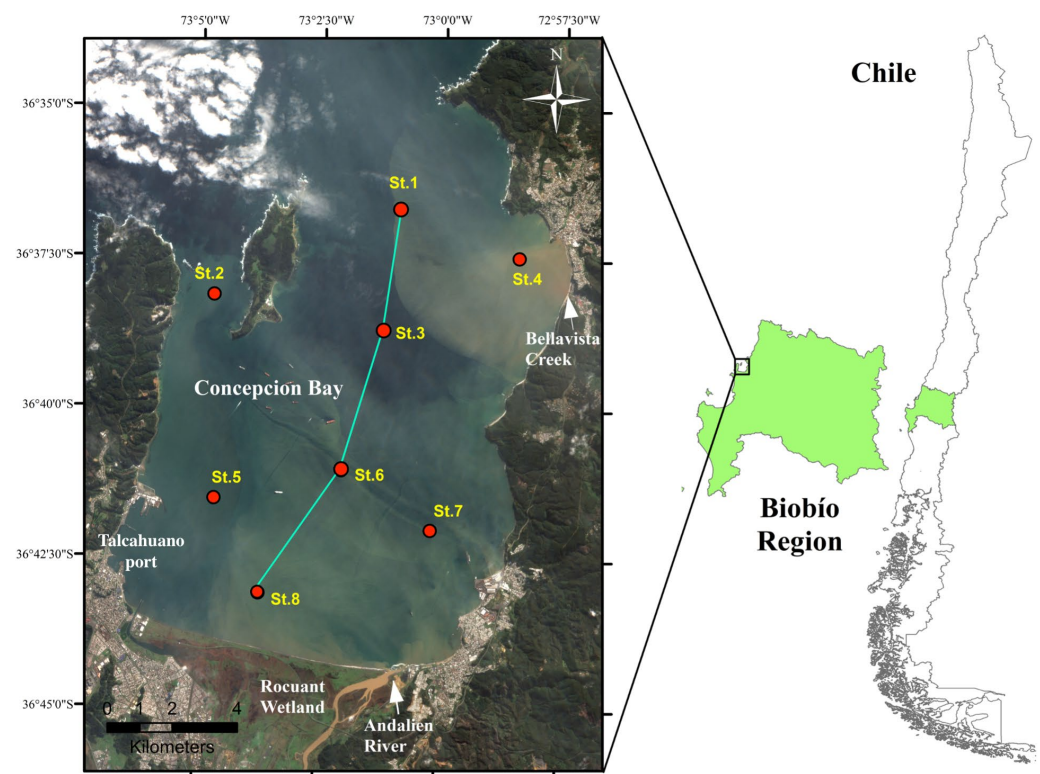

Figure 1. Study area of the Concepción Bay, Biobío Region, Chile. Red dots indicate sampling stations. The green line denotes the meridional transect used in Figure 4 to represent hydrographic spatiotemporal variability. The real color image (Georeferenced MSI/S2) denoted the influence of the plumes of the main tributaries (Andalien River and Bellavista Creek) on the bay. Image obtained from the Copernicus Open Access Hub (https://scihub.copernicus.eu, accessed on 29 May 2018). The product S2MSI1C was obtained from platform 2B. Atmosphere effects were corrected using the Sen2Cor plugin.

Table 1. Summary of the sampling information and methods used in the analyses of physiochemical and biological parameters.

General Information		
Campaign	**Dates**	**Season**
CB 1	3 January 2018	Summer
CB 2	30 May 2018	Fall
CB 3	29 August 2018	Winter
CB 4	29 November 2018	Spring
Measurements per campaign			
Parameters	**Method**	**Parameters**	**Method**
Physicochemical:			
Temperature (°C)	SeaBird SBE−19 plus CTD	Nitrite − NO_2^- (μM)	Standard methods
Salinity (psu)	SeaBird SBE−19 plus CTD	Nitrate − NO_3^- (μM)	Standard methods
Density (sigma-t)	SeaBird SBE−19 plus CTD	Ammonium − NH_4^+ (μM)	Standard methods
Oxygen (mL L^{-1})	SeaBird SBE−19 plus CTD	Hydrogen Sulfide − H_2S (μM)	Spectrophotometry
		Total Suspended Solid − TSS (mg L^{-1})	Standard methods
Biological:			
Chlorophyll-a (mg m^{-3})	Fluorometry		
Total coliforms (MPN 100 mL^{-1})	Standard methods	Bacterioplankton (10^3 cell mL^{-1})	Cytometry
Fecal coliforms (MPN 100 mL^{-1})	Standard methods	Picoeukaryotes (10^3 cell mL^{-1})	Cytometry
Phytoplankton (cell mL^{-1})	Utermöhl		

Table 2. Position and depths of sampling at each station.

Stations	Latitude (South)	Longitude (West)	Maximum Depth (m)	Sampling Depth (m)	
				Surface	Bottom
St. 1	36°36,68′	73°0,89′	34	2	30
St. 2	36°38,13′	73°4,71′	18	2	15
St. 3	36°38,69′	73°1,22′	29	2	25
St. 4	36°37,46′	72°58,43′	22	2	20
St. 5	36°41,52′	73°4,65′	8	2	13
St. 6	36°41,03′	73°2,03′	22	2	18
St. 7	36°42,01′	73°0,17′	19	2	15
St. 8	36°43,09′	73°3,70′	8	2	6

2.2. Atmospheric Analyses

Precipitation data were obtained from the Carriel Sur Airport meteorological station maintained by the Dirección Meteorológica de Chile (DMC—36°46′45″ S 73°37′19″ W). Wind data were obtained from the ERA5 reanalysis product through Copernicus Climate Change Service Information (https://cds.climate.copernicus.eu/cdsapp#!/home, accessed on 6 July 2023). This product has a spatial resolution of 0.25° and has been validated previously for the coastal ocean off Central Chile [38]. We consider daily averages of a box of 3 × 3 pixels right off the mouth of Concepcion Bay for the computation of the alongshore (south–north) wind stress, following Large and Pond [39]. The Ekman transport was computed following Smith [40], as Ek = (τ_γ/ρf) × 1000, where τ_γ is the north component of wind stress, ρ is the water density, and f is the Coriolis parameter, considering 1000 m of coastal extension. A wavelet analysis was performed to identify the dominant cycles of

variability in rainfall and Ekman transport for the period 1966–2019 [41,42]. The annual climatologies for both precipitation and the Ekman transport (1966–2009) were calculated to compare with the annual variability of 2018. We chose the year 2009 as the upper limit of the climatologies, considering it marks the start of the megadrought with dramatic changes in rainfall [43,44] and alongshore winds [45,46] along central-southern Chile. Extreme events of daily precipitation for 2018 were estimated using the index R95, defined as those days when the accumulated precipitation exceeds the 95th percentile of the empirical distribution of rainy days (accumulated precipitation above 1 mm) recommended by the Expert Term on Climate Change Detection and Indices—ETCCDI [47–50]. The mean discharges of the principal streams influencing the freshwater content in the bay (i.e., Andalien river—36°49′0″ S 73°1′59″ W and Bellavista creek—36°38′21″ S 72°57′1″ W) were obtained from two stations (code DGA 08220010 and 08210003) of the Dirección General de Aguas of Chile (DGA) for the study period.

2.3. Hydrographic Analyses

Continuous hydrographic profiles were obtained using a Seabird 19 plus V2 conductivity–temperature–depth profiler (CTD), equipped with oxygen (Seabird 43; accuracy 2% of saturation) and fluorescence sensors (Wet Labs FLRT 3945). Discrete water samples were taken in triplicate at two strata: surface and near the bottom (see maximum depth and depths of each stratus by station in Table 2), using a 5 L Niskin bottle (General Oceanics), to determine: dissolved oxygen (DO), chlorophyll (Chl-a), total suspended solids (TSS), nutrients (i.e., nitrate—NO_3^-, nitrite—NO_2^-, and ammonium—NH_4^+), hydrogen sulfide (H_2S), picoplankton, total and fecal coliforms, and phytoplankton abundances and its size structure. It should be noted that because stratification promotes two well-defined layers during most of the year (see details in the Section 3), this sampling strategy well describes the seasonal and vertical variations of the pelagic system of the CB.

DO concentrations were analyzed in 125 mL glass bottles by the Winkler titration method [51]. In order to obtain the total and size-fractionated Chl-a, i.e., <3, 3–20, >20 μm cell size, seawater was filtered onto combusted (12 h; 450 °C) 0.7, 3.0, and 20 μm glass fiber filters (type GF-F), respectively, and measured by fluorometric analysis (Turner Design AU-10) according to standard procedures [52]. Samples (up to 3 L) of total suspended solids were filtered using combusted GF-F filters (0.7 μm) and analyzed by the 2540-D method [53]. Samples for H_2S were fixed by the addition of saturated $ZnCl_2$ and determined spectrophotometrically with the methylene blue method [54]. Nutrient samples were filtered and frozen until further analysis [53].

Water samples to evaluate picoplankton (i.e., heterotrophic and autotrophic (pigmented) microorganisms, i.e., bacteria, archaea, and picoeukaryotes) and phytoplankton abundances were also taken from the Niskin bottle for both surface and bottom depths. Picoplankton samples (2 mL) were fixed with glutaraldehyde (0.1% final concentration), analyzed by a FACSCalibur flow cytometer (Becton Dickinson, CA, USA), and their abundances were estimated following the procedures described previously [55]. Phytoplankton samples (250 mL) were fixed with acetic acid and Lugol′s iodine solution (2–4% final concentration) and analyzed based on the methodology proposed by Utermölh [56], using a phase-contrast inverted microscope (CKX41SF, Olympus Corporation, Tokyo, Japan). Seawater for total and fecal coliforms was collected in glass autoclaved bottles (250 mL), estimated by the multiple fermentation method according to the methodology described in APHA-AWWA-WPCF [53], and reported as the most probable number (MPN) in 100 mL. All mean values (±SD) of the parameters measured at discrete depths are summarized in Table 3.

Table 3. Mean ± standard deviation of the parameters measured at discrete depths along the water column throughout the seasons studied.

Measurements	Summer CB 1		Fall CB 2		Winter CB 3		Spring CB 4	
	Surface	Bottom	Surface	Bottom	Surface	Bottom	Surface	Bottom
Temperature (°C)	12.80 ± 0.78	10.60 ± 0.79	12.40 ± 0.15	12.42 ± 0.06	11.55 ± 0.10	11.06 ± 0.20	12.22 ± 0.14	11.21 ± 0.47
Salinity (psu)	34.47 ± 0.04	34.51 ± 0.04	33.22 ± 0.33	33.91 ± 0.08	33.93 ± 0.11	34.45 ± 0.21	34.39 ± 0.05	34.50 ± 0.05
Density (Sigma-t)	26.01 ± 0.16	26.46 ± 0.17	25.13 ± 0.24	25.66 ± 0.07	25.84 ± 0.10	26.34 ± 0.19	26.08 ± 0.05	26.35 ± 0.12
Oxygen (mL L^{-1})	5.46 ± 0.88	1.61 ± 1.61	5.51 ± 0.25	4.70 ± 0.44	5.13 ± 0.36	2.72 ± 0.84	4.01 ± 0.95	1.84 ± 1.43
Chlorophyll−a (mg m^{-3})	22.32 ± 5.32	16.77 ± 11.22	3.12 ± 1.41	2.29 ± 0.60	2.44 ± 0.42	2.03 ± 0.75	2.39 ± 2.51	1.47 ± 1.14
Total coliforms (MPN 100 mL^{-1})	12.38 ± 9.88	13.62 ± 18.61	1595.0 ± 2050.32	52.83 ± 61.54	54.20 ± 61.34	37.28 ± 61.83	BDL	BDL
Fecal coliforms (MPN 100 mL^{-1})	2.00 ± 0	14.0 ± 16.97	134.75 ± 149.73	14.61 ± 15.96	9.76 ± 7.58	18.50 ± 26.44	BDL	BDL
NO_2^- (μM)	0.23 ± 0.13	3.33 ± 2.90	0.18 ± 0.03	0.16 ± 0.02	0.19 ± 0.03	0.12 ± 0.07	0.48 ± 0.10	0.43 ± 0.19
NO_3^- (μM)	16.87 ± 0.45	22.5 ± 4.16	12.68 ± 2.34	11.72 ± 1.28	13.76 ± 2.18	12.04 ± 8.57	24.7 ± 2.66	27.22 ± 3.79
NH_4^+ (μM)	5.45 ± 3.03	3.39 ± 1.19	0.94 ± 0.39	1.01 ± 0.40	0.19 ± 0.09	0.15 ± 0.02	1.92 ± 0.50	1.70 ± 0.37
H_2S (μM)	BDL	12.09 ± 0.96	BDL	BDL	BDL	BDL	BDL	BDL
TSS (mg L^{-1})	39.08 ± 4.93	34.91 ± 3.94	12.55 ± 1.79	9.76 ± 1.22	8.37 ± 1.44	10.9 ± 2.34	15.01 ± 5.48	19.4 ± 8.76
Phytoplankton (cell mL^{-1})	1649.00 ± 533.90	813.90 ± 568.00	204.70 ± 96.60	373.50 ± 318.20	600.20 ± 391.10	799.60 ± 341.30	443.60 ± 594.70	289.60 ± 195.10
Bacterioplankton (10^3 cell mL^{-1})	594.30 ± 210.80	637.10 ± 200.90	660.40 ± 301.00	462.40 ± 218.50	1033.00 ± 312.30	544.20 ± 164.40	527.70 ± 110.70	464.10 ± 190.70
Picoeukaryotes (10^3 cell mL^{-1})	BDL	BDL	1.70 ± 0.50	1.10 ± 0.30	11.10 ± 6.40	4.10 ± 3.40	1.80 ± 1.60	0.80 ± 0.70

BDL = below detection limit.

2.4. Statistical Analyses

To identify underlying relationships between the evaluated hydrobiological parameters, as well as segregations and/or clusters among them, a principal component analysis (PCA) was employed. This tool reduces the dimensionality of a data set by keeping the elements that contribute the most to its variance [57]. Furthermore, to evaluate the existence of space-time variations in the environmental variables, an analysis of variance based on multiple permutations (PERMANOVA) was carried out, considering the factors: seasonality (summer, fall, winter, and spring), sampling stations, and stratus (surface and bottom), using the distance matrix of the environmental variables obtained from Euclidean distances of the normalized data, considering 9999 permutations [58]. These analyses were performed using the library Vegan [59] from the software R version 4.3.0 [60].

3. Results

3.1. Meteorological and Hydrological Physical Variability

3.1.1. Ekman Transport

The wavelet analysis of the Ekman transport denoted the persistence of a significant annual cycle (i.e., higher intensity in a 1-year band) (Figure 2a). However, a clear decrease in the average Ekman transport was evident during the fall–winter periods from 2009 onwards (Figure 2b). During 2018, maximum upwelling events (positive values of the Ekman transport in Figure 3a) were recorded during austral spring–summer (September to March). On the contrary, more pulses favorable to downwelling (negative values of the Ekman transport) occurred during the fall and winter. The stronger Ekman transport corresponded to the downwelling event during early July with an onshore transport >100 m^3 s^{-1} (Figure 3a). Nevertheless, several upwelling events occurred during the winter months, although their intensity was, in general, lower than that recorded during the spring–summer. Thus, an intermittency between upwelling and relaxation or inversion pulses (favorable to downwelling) developed between April and December 2018 (Figure 3a). With the exception of the strong downwelling event of early July 2018, the Ekman Transport during 2018 was characterized by frequent upwelling events, especially during the fall–winter, where the curve was mostly above average climatology. Note that the climatology shows that, on

average, the period between May and August is predominantly downwelling-favorable (Figure 3a). Thus, the annual cycle of Ekman transport was not as strong, with marked upwelling and downwelling seasons, as compared with the climatological average.
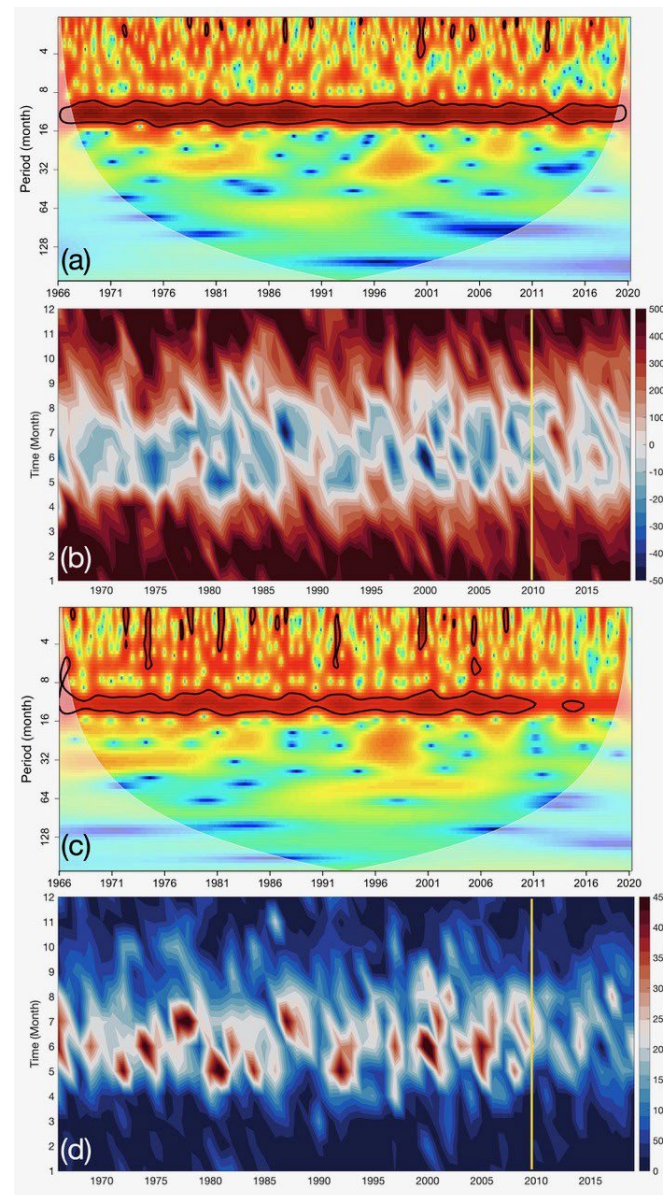

Figure 2. (**a**) Wavelet analysis and (**b**) monthly averages of Ekman transport for the 1966–2019 period. (**c**,**d**) represent the same analysis, respectively, but for precipitation during the same temporal period. Yellow lines indicate the period of a major change in their magnitudes, especially for winters.

3.1.2. Precipitation and River Streamflow

Monthly cumulative precipitation between 1966 and 2019 showed a persistent and significant annual cycle; however, the intensity of this signal decreased from 2009 to 2010 onwards (Figure 2c), which is consistent with a considerable decrement during winter (Figure 2d). The accumulated monthly precipitation recorded for the study area during the sampling period showed a different behavior with respect to the rainfall climatology (1966–2009) (Figure 3b), except for the summer. During austral fall–winter (from May to August), the precipitation values were even lower than the variability (±1 SD) of the climatology, highlighting that the greatest variability of the climatology is observed during these months. In fact, relatively low rainfall occurred during June–August 2018, which

used to be the months with the greatest rainfall of the year in Concepción. In contrast, the maximum rainfall values occurred during the transition periods (i.e., May and September), due to the occurrence of extreme precipitation events. However, the values were within the historical variability, despite being below and above the climatological mean, respectively. Four extreme precipitation events were registered throughout 2018 (arrows in Figure 3c) that oscillated between 30.4 mm (17 September) and 63.6 mm (28 May). It should be noted that the fall sampling (May 30) was carried out just after the maximum precipitation event, which accumulated 111.8 mm in 4 days, corresponding to 14.6% of the total annual rainfall, and consequently, a wide spreading of turbid river plumes influenced the bay (Figure 1).
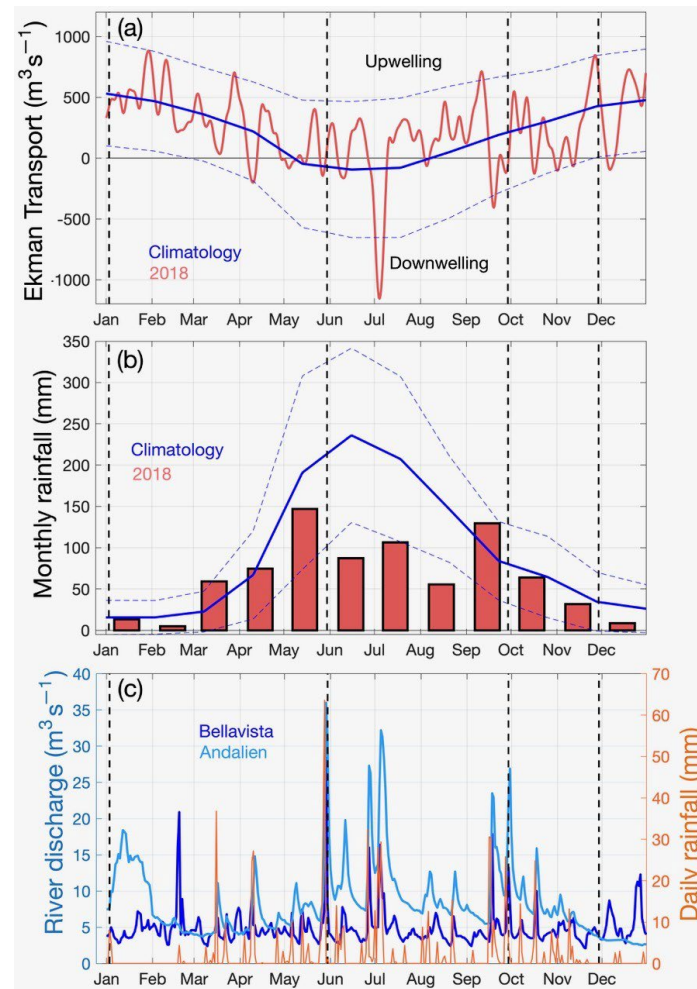

Figure 3. (**a**) Ekman transport (along 1000 m of coast band) for 2018 (red) and the mean climatology (blue curve). Positive (negative) values denote upwelling (downwelling) transport. (**b**) Monthly accumulated precipitation for 2018 (red) and the mean climatology (blue curve). The variability (±1 SD) of the Ekman transport and precipitation climatologies is denoted by horizontal dashed blue lines. (**c**) Daily river discharges for the Andalien River (light blue) and Bellavista Creek (blue) and daily rainfall (orange) are shown for 2018. Vertical dashed lines denote the in situ sampling dates. Red arrows denote peaks of extreme precipitation events during 2018.

3.1.3. Hydrographic Variability and T/S Diagram

Throughout the sampling cruises, the bay remained stratified. During spring and summer, the water column was thermally stratified with a warmer layer fluctuating between the upper 10–15 m depth (Figure 4a,d) and promoting maximum buoyancy frequency at the base of this layer (Figure 4q,t). During fall and winter, the stratification was modulated by the input of freshwater, lowering the salinity of the surface layer (Figure 4f,g). This haline

gradient was remarkably notorious during the fall because the sampling occurred just the day after an extreme rain and discharge event (30 May; Figure 3c). Consequently, maximum buoyancy frequency characterized the surface at ~5 m along the entire north–south axis of the bay (Figure 4r). Thus, the stratification promoting two well-defined layers was always found during our dates of sampling (Figure 4q–t). The spring–summer season was also characterized by the entrance of cold, high-salinity, oxygen-poor waters through the bottom layer (ESSW). During spring and summer, oxygen concentrations fell below the detection limit (<0.5 mL L^{-1}) through most of the water column—from the bottom up to 15 and 10 m depth, respectively (Figure 4i,l). During the upwelling season, the injection of nutrient-rich waters (see Figure 5a) into the photic layer promoted primary production, as evidenced by the subsurface (around 10 m depth) accumulation of Chl-a during the summer (Figure 4m). On the contrary, fall and winter were less productive periods (Figure 4n,o). It is worth noting that an oxygenated water column was captured in fall (Figure 4j), whereas a marked hypoxic (<2.5 mL L^{-1}) bottom layer (down 20 m depth; Figure 4k) was found in winter, possibly due to the input of ESSW (Figure 5c), considering that during this sampling (29 August) and most of August, upwelling-favorable pulses dominated (Figure 3a).
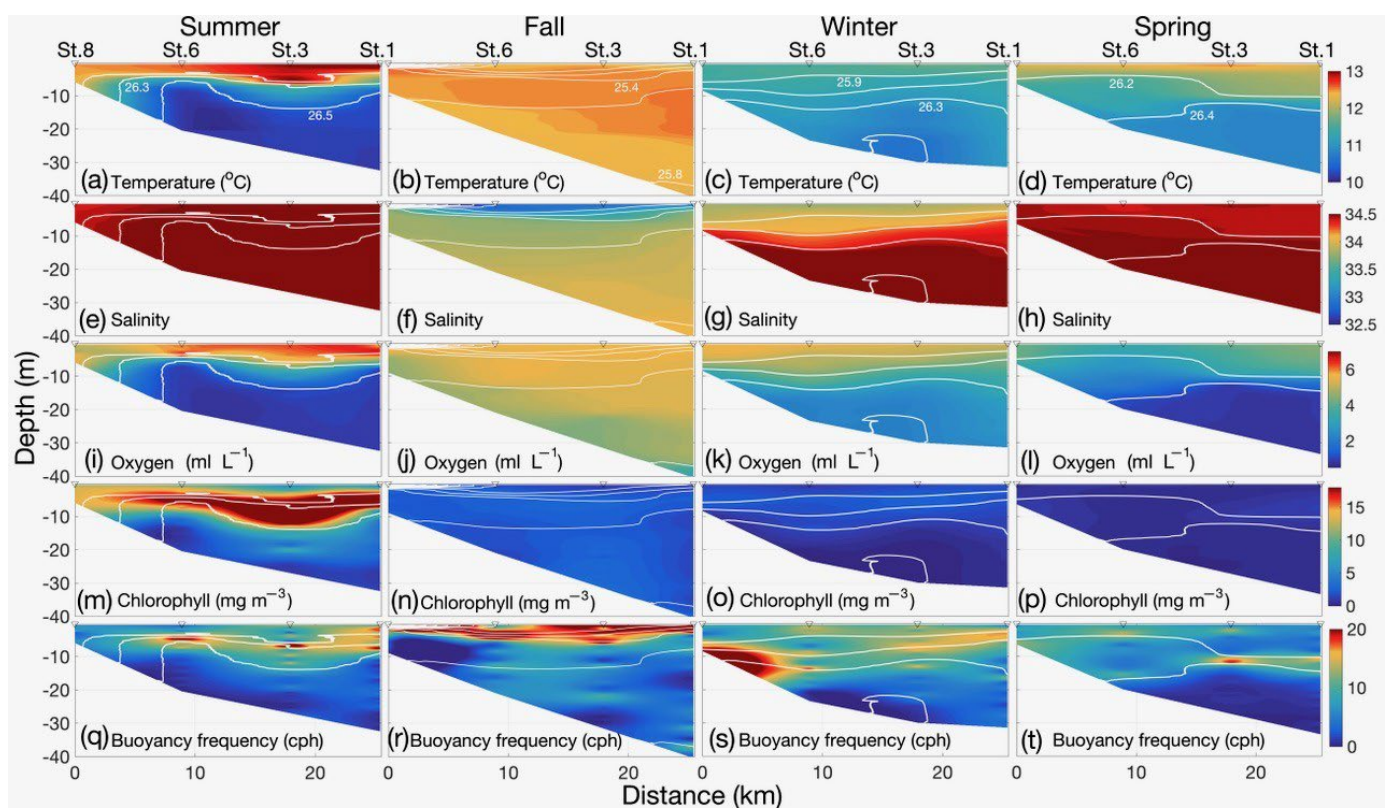

Figure 4. Temporal variability and vertical distribution of temperature (**a–d**), salinity (**e–h**), oxygen (**i–l**), chlorophyll-a (**m–p**), and buoyancy frequency (**q–t**) along a meridional transect (south to north) that considers stations: 8, 6, 3, 1 (see Figure 1) for the sampling seasons: summer (**a,e,i,m,q**), fall (**b,f,j,n,r**), winter (**c,g,k,o,s**), and spring (**d,h,l,p,t**).

During spring–summer (Figure 5a,d), the water column was dominated by waters of equatorial origin, which are characterized by high salinity (34.6), low temperature (11 °C), and low oxygen content (ca. 1.0 mL L^{-1}), typical of the ESSW. The upwelling of this water mass even modified the characteristics of the surface layer, which generally has a subantarctic origin. During the fall (Figure 5b), the water column was dominated by less-salinity (33.7) oxygen-saturated waters (>6.0 mL L^{-1}), characteristic of Subantarctic Waters (SAAW). In winter (Figure 5c), nevertheless, the presence of ESSW was evident along the bottom layer, although the SAAW dominated through most of the water column.
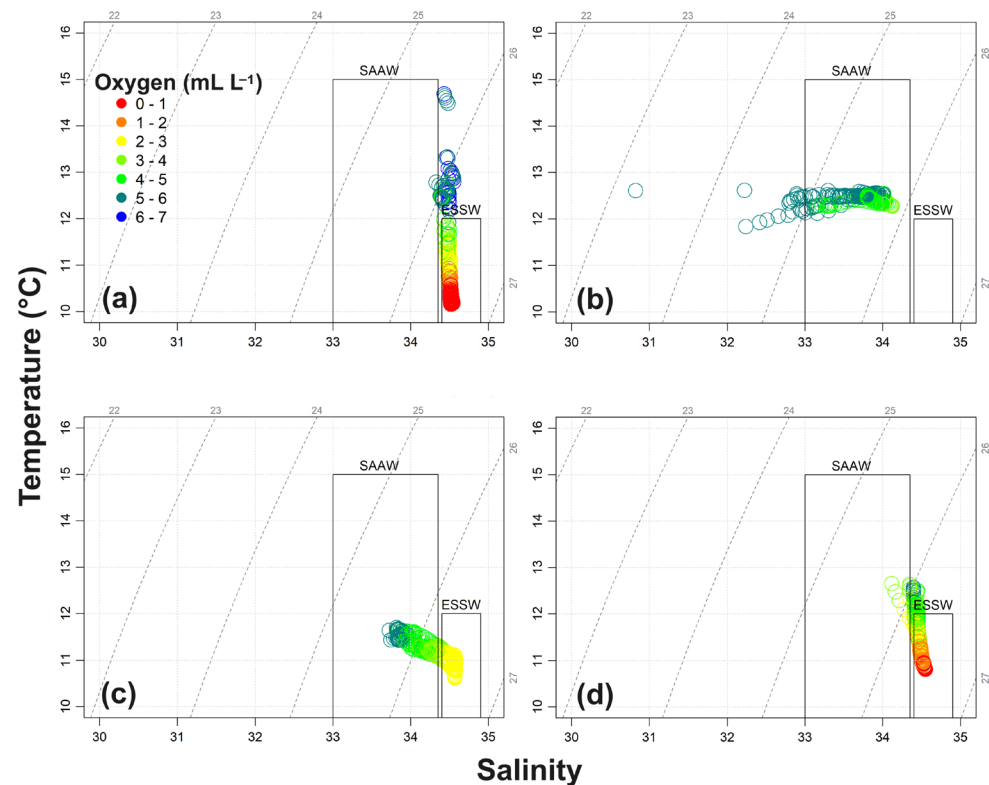
Figure 5. T/S diagrams for the summer (**a**), fall (**b**), winter (**c**), and spring (**d**). Note that the dissolved oxygen variability in the T/S diagrams is represented by the gradient in dot colors. Furthermore, the area with the characteristic values of temperature and salinity corresponding to the main water masses (i.e., SAAW and ESSW) are demarcated by rectangular boxes.

3.2. Biogeochemical Variability

3.2.1. Nutrients and Hydrogen Sulfide (H_2S)

The average nutrient and hydrogen sulfide variability denoted the marked seasonality of the system. Nitrate (Figure 6a) was higher during the upwelling season (i.e., spring and summer), with maximal values in spring for both layers (24.7 ± 2.66 and 27.2 ± 3.79 μM for surface and bottom, respectively), and although its concentrations were reduced at the surface (16.9 ± 0.45 μM) during summer, values at depth remained relatively high (22.5 ± 4.16 μM). Despite lower concentrations found in fall (12.68 ± 2.34 and 11.72 ± 1.28 μM for surface and bottom, respectively) and winter (13.76 ± 2.18 and 11.72 ± 1.28 μM for surface and bottom, respectively) in comparison to the upwelling season, nitrate availability remained relatively high during these periods. Nitrite (Figure 6c) was in general homogenously lower for both layers in fall and winter (<0.2 μM). However, this nutrient was relatively higher in spring (0.48 ± 0.10 μM at the surface and 0.43 ± 0.10 μM at the bottom), reaching its maximum values at depth during summer (3.33 ± 2.90 μM). Similarly, ammonium availability (Figure 6b) was homogenously distributed between the surface (1.92 ± 0.50 μM) and bottom layers (1.70 ± 0.37 μM) during spring, but with concentrations less than half of those found in summer (5.45 ± 3.03 and 3.39 ± 1.19 μM for surface and bottom, respectively), when its maximum accumulation occurred. In contrast, the concentrations of ammonium were lower during fall (0.94 ± 0.39 and 1.01 ± 0.40 μM for surface and bottom, respectively) and winter (0.19 ± 0.09 and 0.15 ± 0.02 μM for surface and bottom, respectively), becoming an order of magnitude smaller in winter than those registered during fall. Hydrogen sulfide (H_2S—Figure 6d) was just registered during summer (readings for other seasons were below detection limit), and its average accumulation occurred particularly at the bottom layer (12.09 ± 0.96 μM), with the greatest concentrations found at the middle (St. 6; 12.77 μM) and middle-west (St. 5; 11.41 μM) of the bay (Supplementary Figure S2).
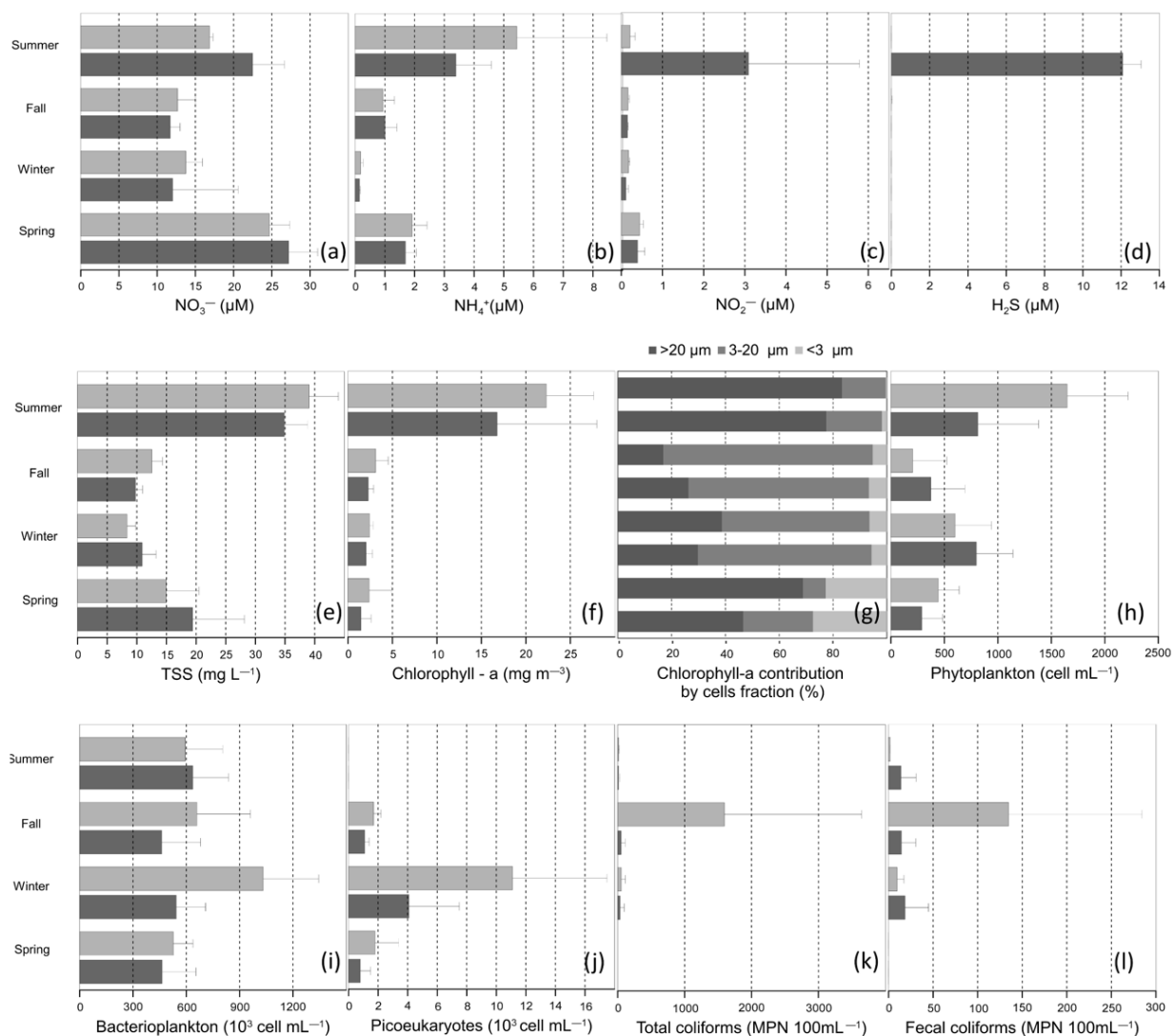
Figure 6. Temporal variability and vertical availability of nitrate (**a**), nitrite (**b**), ammonium (**c**), hydrogen sulfide (**d**), total suspended solids—TSS (**e**), total (**f**) and fractionated (**g**) chlorophyll-a, and abundances of phytoplankton (**h**), bacterioplankton (**i**), picoeukaryotes (**j**), and total (**k**) and fecal (**l**) coliforms. Note that for each season (vertical axis), there are two bars that represent the average values for the surface (light gray) and bottom (dark gray) layers, except for (**g**), where cell fractions are represented by different colors according to the legend on top. In this case, and for each season, the upper bar represents the surface layer, and the lower the bottom ones. Horizontal lines, when corresponding, denote the standard deviation.

3.2.2. Total Suspended Solids and Chlorophyll-a

The concentrations of total suspended solids (TSSs) were higher during the upwelling season (Figure 6e), with slight differences between layers. While the highest mean values were found at depth during the spring (19.4 ± 8.76 mg L^{-1}), a maximum concentration was registered at the surface in summer (39.08 ± 4.93 mg L^{-1}). Oppositely, during the fall and winter, TSS availability was lower, with values < 15 mg L^{-1} more homogeneously distributed through the water column relative to the vertical differences registered during the spring–summer.

The highest chlorophyll-a (Chl-a) concentration was registered during the summer (Figure 6f), reaching peaks ca. 20 mg m^{-3}, mainly concentrated (ca. 80% for both layers) in the cell fraction >20 µm (i.e., chain-forming diatoms). For the other sampling seasons, the concentrations of Chl-a were, in general, lower or just over 5 mg m^{-3}. While the

cell fraction between 3–20 μm dominated (ca. 70% and 60%, respectively) during the fall and winter, being similarly distributed for both layers, in spring, the >20 μm cell fraction was the most represented at the surface (ca. 80%). However, it is remarkable that during the spring, the fraction below 3 μm became important at both layers (ca. 50% in some stations) relative to the other studied periods. The variability of the Chl-a contribution by cell fraction is shown in Figure 6g.

3.2.3. Microbial Community Abundances

Maximum abundances of phytoplankton were registered during summer (Figure 6h), with the highest mean values at the surface (1649.0 ± 533.9 cell mL^{-1}), relative to those found in the bottom layer (813.9 ± 568.0 cell mL^{-1}). Conversely, during the transition periods, i.e., fall and spring, the abundance of phytoplankton was much lower and did not exceed 500 cells mL^{-1}, with higher values at the bottom (373.5 ± 318.2 cell mL^{-1}) and surface (443.6 ± 594.7 cell mL^{-1}) for these periods, respectively. Unexpectedly, phytoplankton abundances in winter were higher relative to the transition periods (600.2 ± 391.1 and 799.6 ± 341.3 cells mL^{-1} for the surface and bottom, respectively). It should be noted that phytoplankton densities were maximum at the surface during the upwelling season (spring and summer), while these peaks were found at the bottom during the fall–winter.

Maximum average abundances of bacterioplankton (i.e., heterotrophic and autotrophic bacteria and archaea) were registered at the surface during the winter ($1033.0 \pm 312.3 \times 10^3$ cells mL^{-1}), denoting a marked difference with the bottom layer ($544.20 \pm 164.4 \times 10^3$ cells mL^{-1}). During the summer, the vertical distribution of picoplankton was more homogeneous, but slightly higher at depth ($637.1 \pm 200.9 \times 10^3$ cells mL^{-1}). Similar densities of bacterioplankton were found at the surface during the summer and fall (ca. 600×10^3 cell mL^{-1}), while lower values (ca. 460×10^3 cell mL^{-1}) were estimated at the deepest layer for the fall and spring (Figure 6i). Picoeukaryotes were also maximum during the winter, relative to the other seasons, and also with clear differences between the surface ($11.1 \pm 6.4 \times 10^3$ cells mL^{-1}) and bottom ($4.1 \pm 3.4 \times 10^3$ cells mL^{-1}) layers, whereas for the transitional periods (i.e., fall and spring), picoeukaryotes densities were similarly lower for both layers ($<2 \times 10^3$ cells mL^{-1}). It is interesting to mention that during the summer, the picoeukaryotes were too low to be detected by the method used (Figure 6j).

The maximum presence of total (1595 ± 2050 MPN 100 mL^{-1}) and fecal (134.8 ± 149.7 MPN 100 mL^{-1}) coliforms was registered at the surface during the fall, with concentrations that exceeded the values estimated for the other seasons by three orders of magnitude (Figure 6k,l, respectively). It should be noted that the fall sampling was carried out just after an extreme rain event (30 May; Figure 3c) and that the distribution of both total and fecal coliforms was more homogeneous throughout the entire bay (see influence of the riverine plumes and of the wetland during this sampling in Figure 1). Although the concentrations of coliforms remained lower during winter and summer, relative to fall conditions, surface values were slightly higher for total coliforms and in an opposite way for fecal coliforms. Nonetheless, despite coliforms concentrations being lower during the winter, higher values were registered both at the surface and bottom in the stations associated with the tributary systems—Bellavista Creek and Andalien River (see Sts. 4 and 7, respectively, in Supplementary Figure S1). It is remarkable that, in general, the coliforms were below the detection limit during the spring.

3.3. Principal Component Analysis

The first component explained 31.2% of the total variability of the data. This variability is modulated by the seasonal changes related to differences in parameters such as salinity, density, nitrate, and total suspended solids, mainly due to the modifications of the water masses in the bay in response to the upwelling process. The second component, explaining 19.9% of the variability, is related to the differences occurring between strata (surface and deepest layers), particularly evident during the summer, mainly because of changes in

temperature, oxygen, Chl-a, ammonium, and phytoplankton abundances, which is related to the high productivity registered during this period (Figure 7).
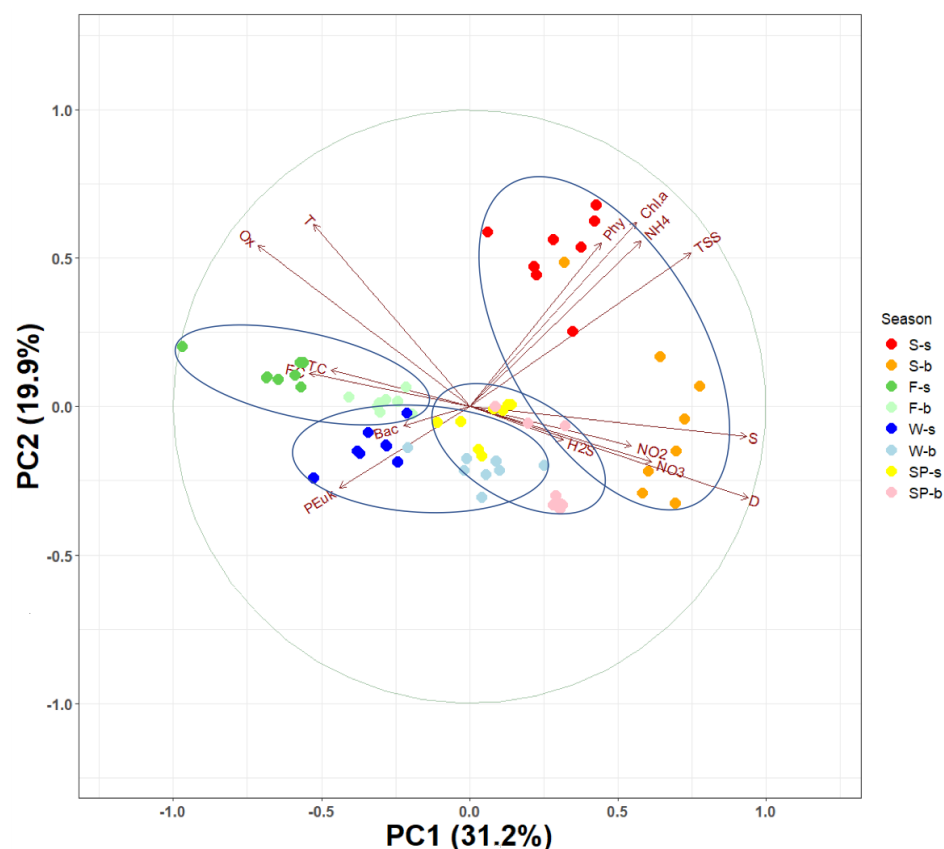

Figure 7. Principal component analysis for the physicochemical and biological parameters evaluated: temperature (T), salinity (S), density (D), oxygen (Ox), nitrate (NO_3), nitrite (NO_2), ammonium (NH_4), hydrogen sulfide (H_2S), total suspended solids (TSS), chlorophyll-a (Chl-a), and abundances of phytoplankton (Phy), bacterioplankton (Bac), picoeukaryotes (PEuk), and total (TC) and fecal (FC) coliforms. Seasons and layers are represented by different colors. Surface (red) and bottom (orange) layers in summer; surface (green) and bottom (light green) layers in fall; surface (blue) and bottom (gray) layers in winter; and surface (yellow) and bottom (pink) layers in spring. The values in parenthesis on each axis indicate the percentage of variance within each principal component/axis.

The PERMANOVA analysis indicates that the Seasonality*Stations and Seasonality*Stratus interactions are significant, while the Stratus*Stations interaction is not (Table 4). Despite the existence of some significant interaction, it is not possible to refer to specific factors determining this interaction. The Seasonality*Stations interaction indicates that the sampling points present significant variations along the different campaigns, denoting that there would be some important local effects (e.g., proximity to the tributaries, presence of a submarine outfall, oceanic or port influence, etc.) affecting the oceanographic conditions at each station. On the other hand, the Seasonality*Stratus interaction is explained due to the differential behavior of some of the parameters evaluated throughout the water column. Thus, there are parameters whose distribution in the water column is modulated by the seasonal changes of the system, while others respond to local effects that are not persistent across all campaigns. Despite the significance of the spatial variations (among sampling stations), the chemical and biological data are presented as averages (standard deviation) for each sampling period (Figure 6), but these variations are discussed in detail where appropriate.

Table 4. Results of the analysis of variance based on multiple permutations (PERMANOVA).

	Df	Sums of Squares	Mean Squares	F. Model	R²	Pr (>F)	
Seasonality	3	17,413,563	5,804,521	8.5158	0.23688	0.001	***
Stratus	1	3,358,419	3,358,419	4.9271	0.04569	0.001	***
Sampling Stations	1	908,203	908,203	1.3324	0.01235	0.286	
Seasonality:Stratus	3	10,656,583	3,552,194	5.2114	0.14496	0.001	***
Seasonality:Stations	3	5,459,898	1,819,966	2.6701	0.07427	0.032	*
Stratus:Stations	1	952,764	952,764	1.3978	0.01296	0.269	
Residuals	51	34,762,614	681,620		0.47288		
Total	63	73,512,045			1		

Significance codes: *** = 0.00; and * = 0.01.

4. Discussion

4.1. Meteorological and Hydrological Temporal Variability

It has been widely established that the alongshore wind forcing modulates the temporal variability of the hydrographic properties, e.g., [61–63], and the coastal marine productivity [64,65] off central-southern Chile. Changes in the wind stress pattern owing to the seasonal cycle in the south-north-south displacement of the South Pacific High (a high atmospheric pressure system), also referred to as South Pacific Anticyclone—SPAc [66], have historically determined two well-defined oceanographic phases: dominance of downwelling in austral fall–winter and upwelling during the spring–summer. As a result, differential hydrographic characteristics modulate the oceanographic regime in CB, with the predominance of SAAW and ESSW in winter and summer, respectively [67–70]. However, the results presented here support a quite different picture of this historical seasonal pattern of the coastal system around 36° S [71], with upwelling-favorable pulses occurring more frequently during the fall–winter, which keep the system stratified and more enriched during most of the year due to the recurrent injection of nutrients. Thus, our study reveals a wind- and rain-modulated change in the temporal behavior of the hydrographic conditions in CB and, consequently, in the biogeochemical response of the system. In this sense, there has been an intensification and southward displacement of the SPAc since 2007 [46], which promotes an intensification of the coastal equatorward winds, and consequently, more upwelling-favorable winds [45,72]. This is particularly relevant in the context of the future of eastern boundary margins under climate change, since the Humboldt Current System would be one of the most affected by the intensification of alongshore winds and the extension of the upwelling season [73]. This increment in the upwelling frequency and strength has substantially cooled the water column and increased the surface salinity of this coastal system, with important changes in the structure (and likely on the function) of the phytoplankton [74] and zooplankton communities [75], and by extension, on higher trophic levels [76]. This concatenated response of the system, due to the change in the regular seasonal dynamics of the upwelling, has great socioeconomic implications considering that CB is a pivotal area for larval retention of important commercial fish species like anchoveta that spawn during winter when environmental conditions are adequate (i.e., low temperature, strong turbulence, and reduced productivity) due to the lack of coastal upwelling and a seasonal light limitation [77,78].

The marine productive yield triggered by coastal upwelling depends not just on nutrient injection but also on the water column stratification, e.g., [79]. Stratification off central-southern Chile, including CB, is mainly modulated by seasonal changes in the heat flux (i.e., insolation) throughout the year and by the buoyancy generated by the river discharge inflow and precipitation during the spring and winter, respectively [62,80]. The conceptualization of the seasonal dynamic in this coastal system establishes that the change in wind stress during fall–winter breaks the stratification generated by the summer upwelling. However, the results obtained here show that CB could function as a two-layer system during most of the year: thermally stratified in spring–summer and by

freshwater flows in fall–winter, with a marked temporal asynchrony between the surface layer and the bottom layer, particularly evident during the fall–winter. Nonetheless, it is important to highlight that the stratification also varies on a synoptic scale in response to the intensification or relaxation of the wind stress [37,81,82]. Thus, rapid temporal changes can occur in the water column structure within a particular season.

Precipitation in southern-central Chile is controlled by the displacement to the most northern position of the SPAc, which allows the entrance of extratropical cold fronts during the winter [83]. However, since the 1950s, a negative trend in annual rainfall has prevailed in this region [84], which has intensified since 2009 due to an unprecedented extreme drought event [43,44]. Changes in the rainfall pattern, which include a diminished precipitation, particularly during winter, and the increasing recurrence and intensification of extreme rainfall events [23–28] during the transitional periods (i.e., fall and spring), have implications for the productivity and sanitary condition (see details below) of this coastal ecosystem. Some of these extreme rainfall events have been identified as atmospheric rivers, which induce heavy orographic precipitation with up to 45–60% of the total annual precipitation in the region between 32° S and 37° S [85]. The changes in the amount and timing of the water delivered have impacts on the stratification, the dilution effect of freshwater inputs, and the amount and quality of the terrigenous materials in the system.

4.2. Seasonal and Vertical Biogeochemical Variability

The biogeochemical variability observed through this study denotes the seasonality of the system in response to the injection of nitrate-rich, oxygen-poor ESSW during the spring–summer. This fertilization enhanced the primary production, especially near the surface, as evidenced by the accumulation of Chl-a and the biomass of phytoplankton. However, a relatively high nitrate concentration remains in the system throughout the year, due to the frequent occurrence of upwelling-favorable intermittent pulses during the fall–winter. This injection of nutrients sustained an active but less abundant photoautotrophic community (relative to summer) composed mainly of small cells (see details of the biological variability below). On the other hand, oxygen concentrations fell below the detection limit (<1 mL L^{-1}) through most of the water column during spring and summer. Considering that the summer sampling occurred just during a wind-relaxation event and after a long period of upwelling-favorable pulses, it is expected that the coupling between surface and deeper layers had been promoted, facilitating organic matter produced by photosynthesis at the surface (using the TSS as a proxy, whose concentration was similarly higher in the surface layer and at the bottom) to settle and be respired at depth [86,87]. These respiration processes not only remineralize the organic material, returning inorganic compounds to the system (e.g., ammonium, nitrite, and nitrate), but also determine the intensity of the oxygen deficiency in the already oxygen-limited waters (i.e., ESSW) that are advected into the shelf (including the CB) during the upwelling pulses [65,88]. Under this oxygen limitation and nitrate availability, microbial-mediated nitrate metabolism is expected to be activated [89,90], and the organic matter should be respired by heterotrophic microorganisms mainly through the reduction of nitrate/nitrite, which act as electron acceptors instead of oxygen, e.g., [91]. These processes generate remineralized ammonium as a product of the decomposition of nitrogenous organic material, evident through the huge accumulation of this compound during the summer. Thus, considering all these geochemical signatures, i.e., oxygen depletion, nitrate availability, and nitrite and ammonium accumulations, it is possible to speculate that nitrogen loss processes are occurring at depth in the central part of the bay (Stations 3, 5, and 6), similarly to what has been reported in a time series station (St. 18) located in the middle shelf (18 nm offshore) off CB [88]. These metabolic pathways, named canonical denitrification, which may include the autotrophic process known as ANAMMOX (anaerobic ammonium oxidation), produce refractory forms of nitrogen such as N$_2$O and/or N$_2$, thus regulating the loss of bio-available nitrogen species, e.g., [91,92]. As a result, it limits the productivity of the system. Furthermore, the N$_2$O produced could eventually diffuse into the atmosphere [93], impacting the climate since it is a powerful

greenhouse gas, 300 times more radiatively effective than CO_2, and a major catalyst for ozone destruction in the stratosphere [94].

It is important to highlight that there was a large accumulation of nitrite (3.33 ± 2.90 μM) but particularly of H_2S (12.09 ± 0.96 μM) in the bottom layer during the summer, evidencing anoxic conditions [95] just in the inner part of the bay (Stations 5 and 6; Supplementary Figure S2). Under this absence of oxygen, H_2S is mainly produced in the sediments (and its interface with the water column) as the result of organic matter degradation through microbial sulfate-reduction processes [96]. Sediments of the bay were characterized by a high content of organic matter (>10%), which has been associated with the eutrophication of this system, i.e., high rates of photoautotrophic primary production and the deposition of the biomass produced, especially during the upwelling season [15,97,98]. During this period, sedimentary sulfate-reduction rates in CB are significantly higher relative to winter [15]. Depending on the mechanisms that control the ventilation at depth (i.e., wind stress, stratification, and water circulation), the H_2S accumulated at the bottom could spread to the water column [99,100]. In this sense, and similar to other highly productive Eastern Boundary Upwelling Systems, such as Namibia and Peru, where sulfidic conditions reach values up to 30 and 4 μmol H_2S L^{-1}, respectively [101,102], the bottom accumulation of H_2S and its subsequent subsurface oxidation to elemental sulfur (S^0) is evident by the presence of turquoise discolored surface waters due to the light reflection produced by the formation of colloidal precipitated microgranules of S^0 [102–104]. A true color Sentinel image revealed the formation of a sizable patch (~50,96 km^2) of milky turquoise waters during the summer, which corresponds to ~30% of the total area of the bay (Supplementary Figure S2). Considering H_2S is a highly toxic gas to most eukaryote organisms, with negative consequences for fisheries and human health [103,105–108], and that pulses of occurrence of these turquoise waters in CB are frequent during the upwelling season [109], the lack of knowledge of its causes and consequences generates concern and uncertainty among the authorities and the population in general. Nevertheless, studies conducted in the vicinity (St. 18) of the CB demonstrated that γ-proteobacteria involved in sulfur cycling (i.e., SUP05) are highly abundant in the bottom waters of this system [110] and that they probably detoxified the waters via the chemolithotrophic oxidation of H_2S coupled to the reduction of NO_3^- [88], in a pathway known as sulfur-driven autotrophic denitrification, similarly to the observed in sulfidic African shelf waters [101].

4.3. Seasonal and Vertical Variability of Biological Communities

It is well known that the main source of energy that sustains the productivity of the marine aquatic ecosystem is phytoplankton, e.g., [111] and references therein. In the Humboldt Current System, the particularly high primary production is mainly promoted by wind-modulated upwelling of nutrient-rich waters [64,86]. This increment in the phytoplankton biomass triggers the heterotrophic activity in the pelagic system [112–114], channeling the energy to higher trophic levels and supporting one of the biggest fisheries worldwide [115–117]. As it was already established, during our hydrographic sampling periods there were upwelling-favorable pulses not just during the spring–summer but also during the fall–winter months, which allowed macronutrient content like nitrate to remain relatively high throughout the year. This wind-forcing fertilization generates remarkable seasonal changes not just in the total mean abundances but also in the structure of the phytoplankton community, as evidenced by the temporal variability of the size-fractioned chlorophyll. Thus, the highest phytoplankton abundance (and Chl-a), mainly represented by micro-phytoplankton cells (>20 μm), was registered, especially at the surface during summer. In contrast, less abundant (two-three times more than the summer) nano-phytoplankton (3–20 μm) cells dominated in the fall–winter period. Analysis of the temporal variability (2002–2009) of the phytoplankton structure at the middle shelf off CB (i.e., St. 18) demonstrated that, at inter-annual scale, total abundance and biomass of the micro-phytoplankton community were at least one order of magnitude greater during the spring–summer [74], varying from neritic chain-forming diatoms during the upwelling

period to pennate sorts typical of coastal waters during the fall–winter [74,118–121]. On the contrary, it seems that there is not a clear seasonality for the nano-phytoplankton community at St. 18 (2004–2006), although the highest mean abundance and biomass were estimated during the upwelling season [118,122]. This temporal variability of phytoplankton, dominated by a few diatom genera, has been related to changes in the upwelling intensity and frequency, but also to changes in surface temperature and salinity [74], which are controlled by the fluctuations of solar radiation throughout the year and by the freshwater input, mainly due to rainfall in the winter and melting from the Biobío river during the spring [62,80]. CB is also thermally stratified during the spring and summer and by the entrance of freshwater during fall and winter, mainly by rain and through the Andalien River and Bellavista Creek. The water stability produced by this thermic and haline stratification and the permanent availability of nutrients generate conditions favorable to phytoplankton development, e.g., [79], although with marked biomass and size (i.e., composition) differences between summer and winter. Nevertheless, it is interesting to highlight that despite the spring sampling occurring once the upwelling season was already developed (i.e., during the second third of the season by the end of November), the system denoted a remarkably lower phytoplankton biomass and Chl-a content than in summer and even than in winter. This lower productivity should be related to the synoptic behavior of the upwelling events, where equatorward winds alternate with periods (2 to 8 days) of relaxation or even reversals [123,124], since the relaxation of the upwelling intensity provides the required steadiness that triggers the phytoplankton bloom [86,87]. Therefore, because the spring sampling occurred at the end of a prolonged active upwelling period (that lasted ~15 days), and despite the fact that the system was full of nutrients (the highest nitrate content both at the surface and bottom of all samplings), it seems that turbulent conditions did not allow phytoplankton to take advantage of this injection of nutrients, evidencing the importance of the balance between physical and nutritional forces for this community [125,126]. During this period, nevertheless, pico-phytoplankton (<3 μm) also became an important fraction of the total Chl-a, with values higher than 20% for the surface and bottom layers, contributing considerably to carbon cycling, as it has been widely demonstrated in coastal systems [127–129], especially when larger phytoplankton (i.e., nano- and micro-plankton) are not blooming [130]. On the contrary, during winter, maximum abundances of bacterioplankton and pico-eukaryotes, relative to the other seasons, indicate that during this period, an important part of the energy is produced through active heterotrophic activity by the remineralization of organic matter and channeled to higher trophic levels by the microbial food web [131], becoming an important source of energy for ciliates and flagellates [119,122,130]. In fact, up to 96% of the primary production could be utilized by the bacterioplankton community in the upwelling areas of the Humboldt Current System off Chile [113]. Changes in the size of the primary producers affect not only the efficiency of energy that is transferred to higher trophic levels but also the sedimentation rates of the organic matter.

On the other hand, a significant contribution of total and fecal coliforms was recorded in the surface waters of CB after the extreme precipitation event registered during the fall sampling. The presence of these bacteria is associated with fecal contamination, an indicator of the potential entry of other pathogens into the system. Hepatitis A outbreaks have been reported in human coastal populations in the study area associated with fecal pollution events that were significantly correlated with an important increase in precipitation [17]. Several studies report the appearance of infectious disease outbreaks after severe weather events, especially rain and floods [132–137]. Therefore, the increase in the frequency and intensity of extreme rain events could affect the water quality of CB with important consequences for public health, considering that it is a multiple-use area where different productive activities coexist (e.g., port, industrial, artisanal, sports, recreational, and touristic), in addition to being a place of spawning, recruitment, and extraction of important marine resources [3–5]. Future studies should consider the residence times of the bay under the effects of high river discharge events and their potential implications

on the accumulation/dispersion of pathogens. Among these resources, bivalve mollusks are of particular interest since they can concentrate several human pathogens transmitted by fecal wastes, including enteric viruses such as Norovirus and hepatitis A virus (HAV) [16,138–140]. Pathogen increments in CB, therefore, could affect the human population through the consumption of these marine commercial species. In fact, reports from the Ministerial Secretary (SEREMI) of Health of the Government of Chile confirmed an increase of 88% in cases of hepatitis A in the Biobío region during the hydrographic sampling period (2018) relative to the previous year, suggesting avoiding the consumption of raw marine species [18,141].

5. Final Considerations

In the actual climatic crisis, several atmospheric and oceanographic stressors are projected [20]. For instance, an intensification of the alongshore upwelling favorable wind stress is projected [35], due to the increment in the temperature and atmospheric pressure gradient between land masses and the ocean [36]. This increment, not just in the upwelling strength but also in its frequency, has changed the structure of the water column off central-southern Chile [46], and the biological response of the system has become evident [74–76]. However, this increment in the upwelling strength would not only occur during the spring–summer but also during the winter [46]. Furthermore, changes in the frequency, intensity, and timing of extreme rainfall events are becoming more recurrent [25,26,28,29]. In this context, our results indicate that changes in the regular pattern of rainfall together with recurrent upwelling-favorable wind pulses during fall–winter altered the seasonality of the physicochemical conditions and the structure of the phyto- and pico-planktonic communities during 2018, with productivity and sanitary implications affecting not just the biogeochemical behavior but the ecosystem functioning of CB.

On the other hand, the frequency and intensity of drastic dissolved oxygen decline (<20 µM O_2) events in many coastal marine environments have increased worldwide since the 1960s [34,142–145]. In fact, a recent long-term study demonstrated the intensification of the hypoxia over the continental shelf off CB, where hypoxic and severe hypoxic waters (<89 and <22 µmol O_2 L^{-1}) have increased more than 2-fold in volume since 1997 [146]. The projected decrease in oxygen concentrations [32] and the increase in water column stratification [33], as well as local eutrophication [34], might lead to more frequent and intense events of oxygen and other electron acceptors (e.g., NO_3^- and NO_2^-) reduction. This would be mainly because of N loss processes, which could also favor the accumulation of toxic sulfide waters in coastal marine systems [99–103], as was registered during 2018 in CB, with consequences that have not yet been clearly defined for the functioning of this coastal marine ecosystem and the sustainability of its resources. These projections in the biogeochemical properties of the upwelling ecosystems (decrease in oxygen content, increased production of greenhouse and noxious gases, changes in composition of primary producers, etc.) agree with the potential changes in other eastern boundary systems worldwide, e.g., [147,148].

Supplementary Materials: The following supporting information can be downloaded at: https://www.mdpi.com/article/10.3390/geosciences14050125/s1, Supplementary Figure S1: Total (left) and fecal (right) coliforms by layers, including all stations sampled during the seasons studied; Supplementary Figure S2: Hydrogen sulfide availability (in µM) at the bottom layer (upper panel) and a true color Sentinel image denoting the influence of turquoise waters at the surface of CB (lower panel) during the summer campaign. The sentinel image was obtained from the Copernicus Open Access Hub (https://scihub.copernicus.eu, accessed on 7 September 2022); the date with the image available corresponds to the sampling time (3 January). It should be noted that even if hydrogen sulfide accumulates in bottom waters, as seen in the upper panel, it is unlikely to be detected by remote sensing until it oxidizes and rises to surface waters. Taking into account that the true color image was obtained during an upwelling pulse (see Figure 2), it is expected that the turquoise-colored waters developed in the southern part of the bay considering the two-layer circulation with a bottom southward inflow during upwelling conditions [149].

References

1. Ahumada, R. Producción y destino de la biomasa fitoplanctónica en un sistema de bahías en Chile central: Una hipótesis. *Biol. Pesq.* **1989**, *18*, 53–66.
2. Djurfeldt, L. Circulation and mixing in a coastal upwelling embayment; Gulf of Arauco, Chile. *Cont. Shelf Res.* **1989**, *9*, 1003–1016. [CrossRef]
3. Cubillos, L.; Arancibia, H. Sobre el crecimiento estacional de la sardina común (*Strangomera bentincki*) y anchoa (Anillo de Engraulis) off Talcahuano, Chile. *Rev. Biol. Mar.* **1993**, *28*, 43–49.
4. Arcos, D. Variabilidad de Pequena Escala En La Zona Neritica Del Sistema de Surgencia de Talcahuano (Chile Central): Identificacion y Dinamica de Aeas de Retencion Larval. *Gayana. Ocean.* **1996**, *4*, 21–58.
5. Castro, L.; Quiñones, R.; Arancibia, H.; Figueroa, D.; Roa, R.; Sobarzo, M.; Retamal, M. *Áreas de Desove de Anchoveta y Sardina Común en la Zona Central*; Informe Final Proyecto Fondo de Investigación Pesquera No. 96-11; Universidad de Concepción: Concepción, Chile, 1997; 115p.
6. Ahumada, R.; Rudolph, A.; Martinez, V. Circulation and fertility of waters in Concepcion Bay. *Estuar. Coast. Shelf Sci.* **1983**, *16*, 95–105.
7. Pantoja, S.; González, H.; Bernal, P.A. Size-fractioned autotrophic production in a shallow bay. *Biol. Pesq.* **1987**, *16*, 99–105.
8. Ahumada, R.; Matra, P.; Silva, N. Phytoplankton biomass distribution and relationship to nutrient enrichment during an upwelling event off Concepcion Bay Chile. *Boletín Soc. Biol. Concepción* **1991**, *62*, 7–19.
9. Brandhorst, W. Condiciones oceanográficas estivales frente a la Costa de Chile. *Rev. Biol. Mar.* **1971**, *14*, 45–84.
10. Arcos, D.F.; Wilson, R.E. Upwelling and the distribution of chlorophyll a within the Bay of Concepción, Chile. *Estuar. Coast. Shelf Sci.* **1984**, *18*, 25–35. [CrossRef]
11. Gómez, V.; Pozo, K.; Nuñez, D.; Přibylová, P.; Audy, O.; Baini, M.; Fossi, M.C.; Klánová, J. Marine plastic debris in Central Chile: Characterization and abundance of macroplastics and burden of persistent organic pollutants (POPs). *Mar. Pollut. Bull.* **2020**, *152*, 110881. [CrossRef]
12. Pozo, K.; Gómez, V.; Přibylová, P.; Lammel, G.; Klánová, J.; Rudolph, A.; Ahumada, R. Multicompartmental analysis of POPs and PAHs in Concepción Bay, central Chile: Part I—Levels and patterns after the 2010 tsunami. *Mar. Pollut. Bull.* **2022**, *174*, 113144. [CrossRef] [PubMed]
13. Pozo, K.; Gómez, V.; Tucca, F.; Galbán-Malagón, C.; Ahumada, R.; Rudolph, A.; Klánová, J.; Lammel, G. Multicompartmental analysis of POPs and PAHs in Concepción Bay, central Chile: Part II—Air-sea exchange during Austral summer. *Mar. Pollut. Bull.* **2022**, *177*, 113518. [CrossRef] [PubMed]

14. Valiela, I. Marine ecological processes. *J. Mar. Biol. Assoc.* **1995**, *76*, 551. [CrossRef]

15. Farias, L. Remineralization and accumulation of organic carbon and nitrogen in marine sediments of eutrophic bays: The case of the Bay of Concepcion, Chile. *Estuar. Coast. Shelf Sci.* **2003**, *57*, 829–841. [CrossRef]

16. Campos, C.J.A.; Avant, J.; Gustar, N.; Lowther, J.; Powell, A.; Stockley, L.; Lees, D.N. Fate of Human Noroviruses in Shellfish and Water Impacted by Frequent Sewage Pollution Events. *Environ. Sci. Technol.* **2015**, *49*, 8377–8385. [CrossRef] [PubMed]

17. González-Saldía, R.R.; Pino-Maureira, N.L.; Muñoz, C.; Soto, L.; Durán, E.; Barra, M.J.; Gutiérrez, S.; Díaz, V.; Saavedra, A. Fecal pollution source tracking and thalassogenic diseases: The temporal-spatial concordance between maximum concentrations of human mitochondrial DNA in seawater and Hepatitis A outbreaks among a coastal population. *Sci. Total Environ.* **2019**, *686*, 158–170. [CrossRef] [PubMed]

18. Sanhueza, G.; Cachicas, V. Detección y cuantificación de virus de hepatitis A en moluscos en las bahías de Concepción y Arauco, Chile. *Rev. Inst. Salud Pública* **2020**, *4*, 10–19. [CrossRef]

19. *EPA 506-6-90-003*; Contaminated Sediments. Relevant Statutes and EPA Program Activities. U.S Environmental Protection Agency, Sediment Oversight Technical Committee: Washington, DC, USA, 1990; p. 158.

20. IPCC. *Global Warming of 1.5 °C. An IPCC Special Report on the Impacts of Global Warming of 1.5 °C above Pre-Industrial Levels and Related Global Greenhouse Gas Emission Pathways, in the Context of Strengthening the Global Response to the Threat of Climate Change, Sustainable Development, and Efforts to Eradicate Poverty*; Masson-Delmotte, V., Zhai, H.-O.P., Pörtner, D., Roberts, J., Skea, P.R., Shukla, A., Pirani, W., Moufouma-Okia, C., Péan, R., Pidcock, S., et al., Eds.; Cambridge University Press: Cambridge, UK; New York, NY, USA, 2018; pp. 3–24. [CrossRef]

21. Seager, R.; Ting, M.; Held, I.; Kushnir, Y.; Lu, J.; Vecchi, G.; Huang, H.-P.; Harnik, N.; Leetmaa, A.; Lau, N.-C.; et al. Model Projections of an Imminent Transition to a More Arid Climate in Southwestern North America. *Science* **2007**, *316*, 1181–1184. [CrossRef] [PubMed]

22. Ummenhofer, C.C.; Meehl, G.A. Extreme weather and climate events with ecological relevance: A review. *Philos. Trans. R. Soc. B Biol. Sci.* **2017**, *372*, 20160135. [CrossRef]

23. Andrys, J.; Kala, J.; Lyons, T.J. Regional climate projections of mean and extreme climate for the southwest of Western Australia (1970–1999 compared to 2030–2059). *Clim. Dyn.* **2017**, *48*, 1723–1747. [CrossRef]

24. Szwed, M. Variability of precipitation in Poland under climate change. *Theor. Appl. Climatol.* **2019**, *135*, 1003–1015. [CrossRef]

25. Berg, P.; Moseley, C.; Haerter, J.O. Strong increase in convective precipitation in response to higher temperatures. *Nat. Geosci.* **2013**, *6*, 181–185. [CrossRef]

26. Boucher, O.; Randall, D.; Artaxo, P.; Bretherton, C.; Feingold, G.; Forster, P.; Stocker, T.F.; Qin, D.; Plattner, G.-K.; Zhang, X.Y. Clouds and aerosols. In *Climate Change 2013: The Physical Science Basis*; Contribution of Working Group I to the Fifth Assessment Report of the Intergovernmental Panel on Climate Change; Cambridge University Press: Cambridge, UK, 2013; pp. 571–657.

27. Kharin, V.V.; Zwiers, F.W.; Zhang, X.; Wehner, M. Changes in temperature and precipitation extremes in the CMIP5 ensemble. *Clim. Chang.* **2013**, *119*, 345–357. [CrossRef]

28. Sillmann, J.; Kharin, V.V.; Zwiers, F.W.; Zhang, X.; Bronaugh, D. Climate extremes indices in the CMIP5 multimodel ensemble: Part 2. Future climate projections. *J. Geophys. Res. Atmos.* **2013**, *118*, 2473–2493. [CrossRef]

29. Fischer, E.M.; Knutti, R. Observed heavy precipitation increase confirms theory and early models. *Nat. Clim. Chang.* **2016**, *6*, 986–991. [CrossRef]

30. Du, H.; Alexander, L.V.; Donat, M.G.; Lippmann, T.; Srivastava, A.; Salinger, J.; Kruger, A.; Choi, G.; He, H.S.; Fujibe, F.; et al. Precipitation from Persistent Extremes is Increasing in Most Regions and Globally. *Geophys. Res. Lett.* **2019**, *46*, 6041–6049. [CrossRef]

31. Myhre, G.; Alterskjær, K.; Stjern, C.W.; Hodnebrog, Ø.; Marelle, L.; Samset, B.H.; Sillmann, J.; Schaller, N.; Fischer, E.; Schulz, M.; et al. Frequency of extreme precipitation increases extensively with event rareness under global warming. *Sci. Rep.* **2019**, *9*, 16063. [CrossRef] [PubMed]

32. Stramma, L.; Johnson, G.C.; Sprintall, J.; Mohrholz, V. Expanding Oxygen-Minimum Zones in the Tropical Oceans. *Science* **2008**, *320*, 655–658. [CrossRef]

33. Li, G.; Cheng, L.; Zhu, J.; Trenberth, K.E.; Mann, M.E.; Abraham, J.P. Increasing ocean stratification over the past half-century. *Nat. Clim. Chang.* **2020**, *10*, 1116–1123. [CrossRef]

34. Diaz, R.J.; Rosenberg, R. Spreading Dead Zones and Consequences for Marine Ecosystems. *Science* **2008**, *321*, 926–929. [CrossRef]

35. Bakun, A. Global Climate Change and Intensification of Coastal Ocean Upwelling. *Science* **1990**, *247*, 198–201. [CrossRef] [PubMed]

36. Sydeman, W.J.; García-Reyes, M.; Schoeman, D.S.; Rykaczewski, R.R.; Thompson, S.A.; Black, B.A.; Bograd, S.J. Climate change and wind intensification in coastal upwelling ecosystems. *Science* **2014**, *345*, 77–80. [CrossRef]

37. Sobarzo, M.B.; Figueroa, D.; Arcos, D.R. The Influence of Winds and Tides in the Formation of Circulation Layers in a Bay, a Case Study: Concepción Bay, Chile. *Estuar. Coast. Shelf Sci.* **1997**, *45*, 729–736. [CrossRef]

38. Wong, Z.; Saldías, G.S.; Largier, J.L.; Strub, P.T.; Sobarzo, M. Surface thermal structure and variability of upwelling shadows in the Gulf of Arauco, Chile. *J. Geophys. Res. Ocean.* **2021**, *126*, e2020JC016194. [CrossRef]

39. Large, W.G.; Pond, S. Open Ocean Momentum Flux Measurements in Moderate to Strong Winds. *J. Phys. Oceanogr.* **1981**, *11*, 324–336. [CrossRef]

40. Smith, R.L. Upwelling. *Oceanogr. Mar. Biol. Annu. Rev.* **1968**, *6*, 11–46.

41. Torrence, C.; Compo, G.P. A practical guide to wavelet analysis. *Bull. Am. Meteorol. Soc.* **1998**, *79*, 61–78. [CrossRef]

42. Cazelles, B.; Chavez, M.; Berteaux, D.; Ménard, F.; Vik, J.O.; Jenouvrier, S.; Stenseth, N.C. Wavelet analysis of ecological time series. *Oecologia* **2008**, *156*, 287–304. [CrossRef]

43. Garreaud, R.D.; Alvarez-Garreton, C.; Barichivich, J.; Boisier, J.P.; Christie, D.; Galleguillos, M.; LeQuesne, C.; McPhee, J.; Zambrano-Bigiarini, M. The 2010–2015 megadrought in central Chile: Impacts on regional hydroclimate and vegetation. *Hydrol. Earth Syst. Sci.* **2017**, *21*, 6307–6327. [CrossRef]

44. Garreaud, R.D.; Boisier, J.P.; Rondanelli, R.; Montecinos, A.; Sepúlveda, H.H.; Veloso-Aguila, D. The Central Chile Mega Drought (2010–2018): A climate dynamics perspective. *Int. J. Climatol.* **2020**, *40*, 421–439. [CrossRef]

45. Saldías, G.S.; Largier, J.L.; Mendes, R.; Pérez-Santos, I.; Vargas, C.A.; Sobarzo, M. Satellite-measured interanual variability of turbid river plumes off central-southern Chile: Spatial patterns and the influence of climate variability. *Prog. Oceanogr.* **2016**, *146*, 212–222. [CrossRef]

46. Schneider, W.; Donoso, D.; Garcés-Vargas, J.; Escribano, R. Water-column cooling and sea surface salinity increase in the upwelling region off central-south Chile driven by a poleward displacement of the South Pacific High. *Prog. Oceanogr.* **2017**, *151*, 38–48. [CrossRef]

47. Donat, M.G.; Peterson, T.C.; Brunet, M.; King, A.D.; Almazroui, M.; Kolli, R.K.; Boucherf, D.; Al-Mulla, A.Y.; Nour, A.Y.; Aly, A.A.; et al. Changes in extreme temperature and precipitation in the Arab region: Long-term trends and variability related to ENSO and NAO. *Int. J. Climatol.* **2014**, *34*, 581–592. [CrossRef]

48. Rao, K.K.; Patwardhan, S.K.; Kulkarni, A.; Kamala, K.; Sabade, S.S.; Kumar, K.K. Projected changes in mean and extreme precipitation indices over India using PRECIS. *Glob. Planet. Chang.* **2014**, *113*, 77–90. [CrossRef]

49. Ren, Z.; Zhang, M.; Wang, S.; Qiang, F.; Zhu, X.; Dong, L. Changes in daily extreme precipitation events in South China from 1961 to 2011. *J. Geogr. Sci.* **2015**, *25*, 58–68. [CrossRef]

50. de los Skansi, M.M.; Brunet, M.; Sigró, J.; Aguilar, E.; Arevalo-Groening, J.A.; Bentancur, O.J.; Geier, Y.R.C.; Amaya, R.L.C.; Jácome, H.; Ramos, A.M.; et al. Warming and wetting signals emerging from analysis of changes in climate extreme indices over South America. *Glob. Planet. Chang.* **2013**, *100*, 295–307. [CrossRef]

51. Carritt, D.E.; Carpenter, J.H. Comparison and Evaluation of Currently Employed Modifications of the Winkler Method for Determining Dissolved Oxygen in Seawater; a NASCO Report. *J. Mar. Res.* **1966**, *24*, 286–318.

52. Parsons, T.; Maita, C.; Lally, C. *A Manual of Chemical and Biological Methods of Seawater Analysis*; Pergamon Press: Oxford, UK, 1984; 173p.

53. *APHA-AWWA-WPCF Standard Methods (9010) for the Examination of Water and Wastewater*, 23rd ed.; American Public Health Association/American Water Works Association/Water Environment Federation: Washington, DC, USA, 2017.

54. Cline, J.D. Spectrophotometric determination of hydrogen sulfide in natural waters. *Limnol. Oceanogr.* **1969**, *14*, 454–458. [CrossRef]

55. Marie, D.; Partensky, F.; Simon, N.; Guillou, L.; Vaulot, D. Protocols in flow cytometry and cell sorting. In *Living Colors*; Diamond, R.A., DeMaggio, S., Eds.; Springer: New York, NY, USA, 2000; pp. 421–454.

56. Utermöhl, H. Zur vervollkommnung der quantitativen phytoplankton-methodik: Mit 1 Tabelle und 15 abbildungen im Text und auf 1 Tafel. *Int. Ver. Theor. Angew. Limnol. Mitteilungen* **1958**, *9*, 1–38. [CrossRef]

57. Mishra, A. Assessment of water quality using principal component analysis: A case study of the river Ganges. *J. Water Chem. Technol.* **2010**, *32*, 227–234. [CrossRef]

58. Anderson, M.J. *Permutational Multivariate Analysis of Variance (PERMANOVA)*; Balakrishnan, N., Colton, T., Everitt, B., Piegorsch, W., Ruggeri, F., Teugels, J.L., Eds.; John Wiley & Sons, Ltd.: Hoboken, NJ, USA, 2017; pp. 1–15. [CrossRef]

59. Oksanen, J.; Guillaume, F.; Kindt, R.; Legendre, P.; Minchin, P.R.; O'Hara, R.B.; Szoecs, E.; Solymos, P.; Stevens, M.H.H.; Wagner, H.H.; et al. Vegan: Community Ecology Package: Ordination, Diversity and Dissimilarities. R Package Version 2.3-0. 2015. Available online: https://www.researchgate.net/publication/311493644_Vegan_commity_ecology_package_R_package_version_23-0 (accessed on 18 April 2019).

60. R Core Team. R: A Language and Environment for Statistical Computing [Computer Software]. R Foundation for Statistical Computing. 2019. Available online: https://www.scirp.org/reference/ReferencesPapers?ReferenceID=2631126 (accessed on 21 January 2019).

61. Strub, P.T.; Mesias, J.M.; Montecino, V.; Rutllant, J.; Salinas, S. Coastal ocean circulation off western South America, In The Sea; Robinson, A.R. , *Brink, K.H., Eds.*; John Wiley: New York, NY, USA, 1998; Volume 11, pp. 273–313.

62. Sobarzo, M.; Bravo, L.; Donoso, D.; Garcés-Vargas, J.; Schneider, W. Coastal upwelling and seasonal cycles that influence the water column over the continental shelf off central Chile. *Prog. Oceanogr.* **2007**, *75*, 363–382. [CrossRef]

63. Morales, C.E.; Hormazabal, S.; Andrade, I.; Correa-Ramirez, M.A. Time-Space Variability of Chlorophyll-a and Associated Physical Variables within the Region off Central-Southern Chile. *Remote Sens.* **2013**, *5*, 5550–5571. [CrossRef]

64. Daneri, G.; Dellarossa, V.; Quiñones, R.; Jacob, B.; Montero, P.; Ulloa, O. Primary production and community respiration in the Humboldt Current System off Chile and associated oceanic areas. *Mar. Ecol. Prog. Ser.* **2000**, *197*, 41–49. [CrossRef]

65. Farías, L.; Fernández, C.; Faúndez, J.; Cornejo, M.; Alcaman, M.E. Chemolithoautotrophic production mediating the cycling of the greenhouse gases N_2O and CH_4 in an upwelling ecosystem. *Biogeosciences* **2009**, *6*, 3053–3069. [CrossRef]

66. Montecino, V.; Paredes, M.A.; Paolini, P.; Rutllant, J. Revisiting chlorophyll data along the coast in north-central Chile, considering multiscale environmental variability. *Rev. Chil. Hist. Nat.* **2006**, *79*, 213–223. [CrossRef]

67. Ahumada, R.; Chuecas, L. Algunas características hidrogramas de la Bahía de Concepción (36′40′S; 73″02′W) y áreas adyacentes Chile. *Gayana Myscelánea* **1979**, *8*, 1–56.

68. Sobarzo, M. Caracterización de la Circulación de Bahía Concepción, Chile: Un análisis temporal en el dominio de la frecuencia. Ph.D. Thesis, Tesis de Grado de Magister en Ciencias mención Oceanografía, Universidad de Concepción, Departamento de Oceanografía, Concepción, Chile, 1993.

69. Sobarzo, M. Oceanografía Física entre Punta Nugurne (35°57′S; 72°47′W) y Punta Manuel (38°30′S; 73°31′W), Chile: Una revisión histórica (1936–1990). *Gayana Oceanol.* **1994**, *2*, 5–17.

70. Arcos, D.; Núñez, S.; Urrutia, A.; Chuecas, L. Shelf-embayment water exchange and residence times within Concepcion Bay, Chile. *Gayana Oceanol.* **1995**, *3*, 75–87.

71. Montencino, V.; Lange, C. The Humboldt Current System: Ecosystem components and processes, fisheries, and sediment studies. *Prog. Oceanogr.* **2009**, *83*, 65–79. [CrossRef]

72. Belmadani, A.; Echevin, V.; Codron, F.; Takahashi, K.; Junquas, C. What dynamics drive future wind scenarios for coastal upwelling off Peru and Chile? *Clim. Dyn.* **2014**, *43*, 1893–1914. [CrossRef]

73. Wang, D.; Gouhier, T.C.; Menge, B.A.; Ganguly, A.R. Intensification and spatial homogenization of coastal upwelling under climate change. *Nature* **2015**, *518*, 390–394. [CrossRef] [PubMed]

74. Anabalón, V.; Morales, C.E.; González, H.E.; Menschel, E.; Schneider, W.; Hormazabal, S.; Valencia, L.; Escribano, R. Microphytoplankton community structure in the coastal upwelling zone off Concepción (central Chile): Annual and inter-annual fluctuations in a highly dynamic environment. *Prog. Oceanogr.* **2016**, *149*, 174–188. [CrossRef]

75. Medellín-Mora, J.; Escribano, R.; Schneider, W. Community response of zooplankton to oceanographic changes (2002–2012) in the central/southern upwelling system of Chile. *Prog. Oceanogr.* **2016**, *142*, 17–29. [CrossRef]

76. Castro, L.R.; Claramunt, G.; González, H.E.; Krautz, M.C.; Llanos-Rivera, A.; Méndez, J.; Schneider, W.; Soto, S. Fatty acids in eggs of anchoveta *Engraulis ringens* during two contrasting winter spawning seasons. *Mar. Ecol. Prog. Ser.* **2010**, *420*, 193–205. [CrossRef]

77. Castro, L.R.; Salinas, G.R.; Hernández, E.H. Environmental influences on winter spawning of the anchoveta *Engraulis ringens* off central Chile. *Mar. Ecol. Prog. Ser.* **2000**, *197*, 247–258. [CrossRef]

78. Castro, L.R. Environmental conditions and larval survival during the winter spawning season of the southernmost anchoveta stock off Chile. *Globec. Newsl.* **2001**, *7*, 15–17.

79. Gilbert, P.M. Margalef revisited: A new phytoplankton mandala incorporating twelve dimensions, including nutritional physiology. *Harmful Algae* **2016**, *55*, 25–30. [CrossRef] [PubMed]

80. Saldías, G.S.; Sobarzo, M.; Largier, J.; Moffat, C.; Letelier, R. Seasonal variability of turbid river plumes off central Chile based on high-resolution MODIS imagery. *Remote Sens. Environ.* **2012**, *123*, 220–233. [CrossRef]

81. Garreaud, R.; Rutllant, J.; Fuenzalida, H. Coastal Lows along the Subtropical West Coast of South America: Mean Structure and Evolution. *Mon. Weather Rev.* **2002**, *130*, 75–88. [CrossRef]

82. Garreaud, R.D. The Andes climate and weather. *Adv. Geosci.* **2009**, *22*, 3–11. [CrossRef]

83. Montecinos, A.; Aceituno, P. Seasonality of the ENSO-Related Rainfall Variability in Central Chile and Associated Circulation Anomalies. *J. Clim.* **2003**, *16*, 281–296. [CrossRef]

84. Quintana, J.M.; Aceituno, P. Changes in the rainfall regime along the extratropical west coast of South America (Chile): 30–43° S. *Atmósfera* **2012**, *25*, 1–22.

85. Viale, M.; Valenzuela, R.; Garreaud, R.; Ralph, F.M. Impacts of atmospheric rivers on precipitacion in southern South America. *J. Hydrometeorol.* **2018**, *19*, 1671–1687. [CrossRef]

86. Daneri, G.; Lizárraga, L.; Montero, P.; González, H.E.; Tapia, F.J. Wind forcing and short-term variability of phytoplankton and heterotrophic bacterioplankton in the coastal zone of the Concepción upwelling system (Central Chile). *Prog. Oceanogr.* **2012**, *92*, 92–96. [CrossRef]

87. Galán, A.; Zirbel, M.J.; Saldías, G.S.; Chan, F.; Letelier, R. The role of upwelling intermittence in the development of hypoxia and nitrogen loss over the Oregon shelf. *J. Mar. Syst.* **2020**, *207*, 103342. [CrossRef]

88. Galán, A.; Faúndez, J.; Thamdrup, B.; Santibáñez, J.F.; Farías, L. Temporal dynamics of nitrogen loss in the coastal upwelling ecosystem off central Chile: Evidence of autotrophic denitrification through sulfide oxidation. *Limnol. Oceanogr.* **2014**, *59*, 1865–1878. [CrossRef]

89. Devol, A.H. Bacterial oxygen uptake kinetics as related to biological processes in oxygen deficient zones of the oceans. *Deep Sea Res.* **1978**, *25*, 137–146. [CrossRef]

90. Devol, A.H. Solution to a marine mystery. *Nature* **2003**, *422*, 575–576. [CrossRef]

91. Zehr, J.P.; Kudela, R.M. Nitrogen Cycle of the Open Ocean: From Genes to Ecosystems. *Annu. Rev. Mar. Sci.* **2011**, *3*, 197–225. [CrossRef]

92. Lam, P.; Kuypers, M.M.M. Microbial Nitrogen Cycling Processes in Oxygen Minimum Zones. *Annu. Rev. Mar. Sci.* **2011**, *3*, 317–345. [CrossRef]

93. Cornejo, M.; Farías, L.; Gallegos, M. Seasonal cycle of N$_2$O vertical distribution and air–sea fluxes over the continental shelf waters off central Chile (~36°S). *Prog. Oceanogr.* **2007**, *75*, 383–395. [CrossRef]

94. Stein, L.Y.; Yung, Y.L. Production, isotopic composition, and atmospheric fate of biologically produced nitrous oxide. *Annu. Rev. Earth Planet. Sci.* **2003**, *31*, 329–356. [CrossRef]

95. Ulloa, O.; Canfield, D.E.; DeLong, E.F.; Letelier, R.M.; Stewart, F.J. Microbial oceanography of anoxic oxygen minimum zones. *Proc. Natl. Acad. Sci. USA* **2012**, *109*, 15996–16003. [CrossRef] [PubMed]

96. Jørgensen, B.B.; Postgate, J.R.; Postgate, J.R.; Kelly, D.P. Ecology of the bacteria of the sulphur cycle with special reference to anoxic—Oxic interface environments. *Philos. Trans. R. Soc. Lond. B Biol. Sci.* **1982**, *298*, 543–561. [CrossRef] [PubMed]

97. Graco, M.; Farías, L.; Molina, V.; Gutiérrez, D.; Nielsen, L.P. Massive developments of microbial mats following phytoplankton blooms in a naturally eutrophic bay: Implications for nitrogen cycling. *Limnol. Oceanogr.* **2001**, *46*, 821–832. [CrossRef]

98. Graco, M.; Gutiérrez, D.; Farías, L. Inter-annual variability of the Pelagic-Benthic coupling in the upwelling system off central Chile. *Adv. Geosci.* **2006**, *6*, 127–132. [CrossRef]

99. Brüchert, V.; Currie, B.; Peard, K.R. Hydrogen sulphide and methane emissions on the central Namibian shelf. *Prog. Oceanogr.* **2009**, *83*, 169–179. [CrossRef]

100. Dale, A.W.; Sommer, S.; Lomnitz, U.; Bourbonnais, A.; Wallmann, K. Biological nitrate transport in sediments on the Peruvian margin mitigates benthic sulfide emissions and drives pelagic N loss during stagnation events. *Deep Sea Res. Part I Oceanogr. Res. Pap.* **2016**, *112*, 123–136. [CrossRef]

101. Lavik, G.; Stührmann, T.; Brüchert, V.; Van der Plas, A.; Mohrholz, V.; Lam, P.; Mußmann, M.; Fuchs, B.M.; Amann, R.; Lass, U.; et al. Detoxification of sulphidic African shelf waters by blooming chemolithotrophs. *Nature* **2009**, *457*, 581–584. [CrossRef]

102. Schunck, H.; Lavik, G.; Desai, D.K.; Großkopf, T.; Kalvelage, T.; Löscher, C.R.; Paulmier, A.; Contreras, S.; Siegel, H.; Holtappels, M.; et al. Giant Hydrogen Sulfide Plume in the Oxygen Minimum Zone off Peru Supports Chemolithoautotrophy. *PLoS ONE* **2013**, *8*, e68661. [CrossRef]

103. Weeks, S.J.; Currie, B.; Bakun, A. Massive emissions of toxic gas in the Atlantic. *Nature* **2002**, *415*, 493–494. [CrossRef] [PubMed]

104. Ohde, T.; Siegel, H.; Reißmann, J.; Gerth, M. Identification and investigation of sulphur plumes along the Namibian coast using the MERIS sensor. *Cont. Shelf Res.* **2007**, *27*, 744–756. [CrossRef]

105. Copenhagen, W.J. The periodic mortality of fish in the Walvis region. *S. Afr. J. Sci.* **1953**, *49*, 330.

106. Hart, T.J.; Currie, R.I. The Benguela Current. In *Discovery Report 31*; Cambridge University Press: Cambridge, UK, 1960; pp. 123–298.

107. Reiffenstein, R.J.; Hulbert, W.C.; Roth, S.H. Toxicology of hydrogen sulfide. *Annu. Rev. Pharmacol. Toxicol.* **1992**, *32*, 109–134. [CrossRef]

108. Hamukuaya, H.; O'Toole, M.J.; Woodhead, P.M.J. Observations of severe hypoxia and offshore displacement of Cape hake over the Namibian shelf in 1994. *S. Afr. J. Mar. Sci.* **1998**, *19*, 57–59. [CrossRef]

109. Gallardo, V.A.; Espinoza, C. The evolution of ocean color. *Instrum. Methods Mission. Astrobiol. XI* **2008**, *7097*, 128–134. [CrossRef]

110. Murillo, A.A.; Ramírez-Flandes, S.; DeLong, E.F.; Ulloa, O. Enhanced metabolic versatility of planktonic sulfur-oxidizing γ-proteobacteria in an oxygen-deficient coastal ecosystem. *Front. Mar. Sci.* **2014**, *1*, 18. [CrossRef]

111. Field, C.B.; Behrenfeld, M.J.; Randerson, J.T.; Falkowski, P. Primary Production of the Biosphere: Integrating Terrestrial and Oceanic Components. *Science* **1998**, *281*, 237–240. [CrossRef] [PubMed]

112. Barbosa, A.B.; Galvão, H.M.; Mendes, P.A.; Álvarez-Salgado, X.A.; Figueiras, F.G.; Joint, I. Short-term variability of heterotrophic bacterioplankton during upwelling off the NW Iberian margin. *Prog. Oceanogr.* **2001**, *51*, 339–359. [CrossRef]

113. Troncoso, V.A.; Daneri, G.; Cuevas, L.A.; Jacob, B.; Montero, P. Bacterial carbon flow in the Humboldt Current System off Chile. *Mar. Ecol. Prog. Ser.* **2003**, *250*, 1–12. [CrossRef]

114. Cuevas, L.A.; Daneri, G.; Jacob, B.; Montero, P. Microbial abundance and activity in the seasonal upwelling area off Concepción (~36°S), central Chile: A comparison of upwelling and non-upwelling conditions. *Deep Sea Res. Part II Top. Stud. Oceanogr.* **2004**, *51*, 2427–2440. [CrossRef]

115. Cubillos, L.; Núñez, S.; Arcos, D. Primary production required to sustain the Chilean pelagic fisheries. *Investig. Mar.* **1998**, *26*, 83–96.

116. FAO. FAO Yearbooks. Fishery and Aquaculture Statistics. Fisheries and Aquaculture Information and Statistics Service. Fishery and Aquaculture Economics and Policy Division. 2070–6057. 2006. Available online: https://www.fao.org/fishery/fr/publications/51136 (accessed on 9 October 2022).

117. Chavez, F.P.; Bertrand, A.; Guevara-Carrasco, R.; Soler, P.; Csirke, J. The northern Humboldt Current System: Brief history, present status and a view towards the future. *Prog. Oceanogr.* **2008**, *79*, 95–105. [CrossRef]

118. Anabalón, V.; Morales, C.E.; Escribano, R.; Varas, M. The contribution of nano- and micro-planktonic assemblages in the surface layer (0–30 m) under different hydrographic conditions in the upwelling area off Concepción, central Chile. *Prog. Oceanogr.* **2007**, *75*, 396–414. [CrossRef]

119. González, H.E.; Menschel, E.; Aparicio, C.; Barría, C. Spatial and temporal variability of microplankton and detritus, and their export to the shelf sediments in the upwelling area off Concepción, Chile (~36°S), during 2002–2005. *Prog. Oceanogr.* **2007**, *75*, 435–451. [CrossRef]

120. Morales, C.E.; González, H.E.; Hormazabal, S.E.; Yuras, G.; Letelier, J.; Castro, L.R. The distribution of chlorophyll-a and dominant planktonic components in the coastal transition zone off Concepción, central Chile, during different oceanographic conditions. *Prog. Oceanogr.* **2007**, *75*, 452–469. [CrossRef]

121. Sánchez, G.E.; Lange, C.B.; González, H.E.; Vargas, G.; Muñoz, P.; Cisternas, C.; Pantoja, S. Siliceous microorganisms in the upwelling center off Concepción, Chile (36°S): Preservation in surface sediments and downcore fluctuations during the past ~150 years. *Prog. Oceanogr.* **2012**, *92–95*, 50–65. [CrossRef]

122. Böttjer, D.; Morales, C.E. Nanoplanktonic assemblages in the upwelling area off Concepción (~36°S), central Chile: Abundance, biomass, and grazing potential during the annual cycle. *Prog. Oceanogr.* **2007**, *75*, 415–434. [CrossRef]

123. Peterson, W.T.; Arcos, D.F.; McManus, G.H.; Dam, H.; Bellantoni, D.; Johnson, T.; Tiselius, P. The nearshore zone during coastal upwelling: Daily variability and coupling between primary and secondary production off central Chile. *Prog. Oceanogr.* **1998**, *20*, 1–40. [CrossRef]

124. Sobarzo, M.; Djurfeldt, L. Coastal upwelling process on a continental shelf limited by submarine canyons, Concepción, central Chile. *J. Geophys. Res. Ocean.* **2004**, *109*, C12012. [CrossRef]

125. Margalef, R. Phytoplankton communities in upwelling areas. The example of NW Africa. *Oecologia Aquat.* **1978**, *3*, 97–132.

126. Margalef, R. The organization of space. *Oikos* **1979**, *33*, 152–159. [CrossRef]

127. Bec, B.; Husseini-Ratrema, J.; Collos, Y.; Souchu, P.; Vaquer, A. Phytoplankton seasonal dynamics in a Mediterranean coastal lagoon: Emphasis on the picoeukaryote community. *J. Plankton Res.* **2005**, *27*, 881–894. [CrossRef]

128. Worden, A.Z.; Nolan, J.K.; Palenik, B. Assessing the dynamics and ecology of marine picophytoplankton: The importance of the eukaryotic component. *Limnol. Oceanogr.* **2004**, *49*, 168–179. [CrossRef]

129. Collado-Fabbri, S.; Vaulot, D.; Ulloa, O. Structure and seasonal dynamics of the eukaryotic picophytoplankton community in a wind-driven coastal upwelling ecosystem. *Limnol. Oceanogr.* **2011**, *56*, 2334–2346. [CrossRef]

130. Vargas, C.A.; Martínez, R.A.; Cuevas, L.A.; Pavez, M.A.; Cartes, C.; González, H.E.; Escribano, R.; Daneri, G. The relative importance of microbial and classical food webs in a highly productive coastal upwelling area. *Limnol. Oceanogr.* **2007**, *52*, 1495–1510. [CrossRef]

131. Azam, F.; Fenchel, T.; Field, J.G.; Gray, J.S.; Meyer-Reil, L.A.; Thingstad, F. The Ecological Role of Water-Column Microbes in the Sea. *Mar. Ecol. Prog. Ser.* **1983**, *10*, 257–263. [CrossRef]

132. Santo Domingo, J.; Edge, T. Identification of primary sources of fecal pollution. In *Safe Management of Shellfish and Harvest Waters*; Rees, G., Pond, K., Kay, D., Bartram, J., Santo Domingo, J., Eds.; IWA Publishing: London, UK, 2010; pp. 51–90.

133. Rodríguez, R.A.; Gundy, P.M.; Rijal, G.K.; Gerba, C.P. The Impact of Combined Sewage Overflows on the Viral Contamination of Receiving Waters. *Food Environ. Virol.* **2012**, *4*, 34–40. [CrossRef]

134. WHO. World Health Organization position paper on hepatitis A vaccines—June 2012. *Wkly. Epidemiol. Rec. Relev. Épidémiologique Hebd.* **2012**, *87*, 261–276.

135. Hata, A.; Katayama, H.; Kojima, K.; Sano, S.; Kasuga, I.; Kitajima, M.; Furumai, H. Effects of rainfall events on the occurrence and detection efficiency of viruses in river water impacted by combined sewer overflows. *Sci. Total Environ.* **2014**, *468–469*, 757–763. [CrossRef]

136. Suffredini, E.; Proroga, Y.T.R.; Di Pasquale, S.; Di Maro, O.; Losardo, M.; Cozzi, L.; Capuano, F.; De Medici, D. Occurrence and Trend of Hepatitis A Virus in Bivalve Molluscs Production Areas Following a Contamination Event. *Food Environ. Virol.* **2017**, *9*, 423–433. [CrossRef] [PubMed]

137. Tall, J.A.; Gatton, M.L. Flooding and Arboviral Disease: Predicting Ross River Virus Disease Outbreaks across Inland Regions of South-Eastern Australia. *J. Med. Entomol.* **2020**, *57*, 241–251. [CrossRef] [PubMed]

138. Griffin, D.W.; Donaldson, K.A.; Paul, J.H.; Rose, J.B. Pathogenic Human Viruses in Coastal Waters. *Clin. Microbiol. Rev.* **2003**, *16*, 129–143. [CrossRef] [PubMed]

139. Grodzki, M.; Ollivier, J.; Le Saux, J.C.; Piquet, J.C.; Noyer, M.; Le Guyader, F.S. Impact of Xynthia tempest on Viral Contamination of Shellfish. *Appl. Environ. Microbiol.* **2012**, *78*, 3508–3511. [CrossRef] [PubMed]

140. Campos, C.J.A.; Lees, D.N. Environmental Transmission of Human Noroviruses in Shellfish Waters. *Appl. Environ. Microbiol.* **2014**, *80*, 3552–3561. [CrossRef] [PubMed]

141. Ministerio de Salud de Chile. Boletín Epidemiológico Trimestral, Hepatitis A SE 1–52, 2019. Departamento de Epidemiología. Available online: http://epi.minsal.cl/wp-content/uploads/2020/01/BET_HEPATITIS_2019.pdf (accessed on 10 March 2022).

142. Diaz, R.J. Overview of Hypoxia around the World. *J. Environ. Qual.* **2001**, *30*, 275–281. [CrossRef] [PubMed]

143. Wright, J.J.; Konwar, K.M.; Hallam, S.J. Microbial ecology of expanding oxygen minimum zones. *Nat. Rev. Microbiol.* **2012**, *10*, 381–394. [CrossRef] [PubMed]

144. Schmidtko, S.; Stramma, L.; Visbeck, M. Decline in global oceanic oxygen content during the past five decades. *Nature* **2017**, *542*, 335–339. [CrossRef] [PubMed]

145. Breitburg, D.; Levin, L.A.; Oschlies, A.; Grégoire, M.; Chavez, F.P.; Conley, D.J.; Garçon, V.; Gilbert, D.; Gutiérrez, D.; Isensee, K.; et al. Declining oxygen in the global ocean and coastal waters. *Science* **2018**, *359*, eaam7240. [CrossRef]

146. De La Maza, L.; Farías, L. The intensification of coastal hypoxia off central Chile: Long term and high frequency variability. *Front. Earth Sci.* **2023**, *10*, 929271. [CrossRef]

147. Bakun, A.; Black, B.A.; Bograd, S.J.; García-Reyes, M.; Miller, A.J.; Rykaczewski, R.R.; Sydeman, W.J. Anticipated effects of climate change on coastal upwelling ecosystems. *Curr. Clim. Chang. Rep.* **2015**, *1*, 85–93. [CrossRef]

148. Capone, D.G.; Hutchins, D.A. Microbial biogeochemistry of coastal upwelling regimes in a changing ocean. *Nat. Geosci.* **2013**, *6*, 711–717. [CrossRef]

149. Valle-Levinson, A.; Schneider, W.; Sobarzo, M.; Bello, M.; Bravo, L.; Castillo, M.; Duarte, L.; Fuenzalida, R.; Gallegos, J.M.; Garcés, J.; et al. Wind-induced exchange at the entrance to Concepción Bay, an equatorward facing embayment in central Chile. *Deep Sea Res. Part II Top. Stud. Oceanogr.* **2004**, *51*, 2371–2388. [CrossRef]